

1 **CHANS-SD-YRB V1.0: A System Dynamics model of**
2 **the coupled human-natural systems for the Yellow**
3 **River Basin**

4 Shan Sang^{1,2}, Yan Li^{1,2*}, Shuang Zong^{1,2}, Lu Yu^{1,2}, Shuai Wang^{1,2}, Yanxu Liu^{1,2},
5 Xutong Wu^{1,2}, Shuang Song^{1,2}, Wenwu Zhao^{1,2}, Xuhui Wang³, Bojie Fu⁴

6 ¹State Key Laboratory of Earth Surface Processes and Hazards Risk Governance (ESPHR), Beijing
7 Normal University, Beijing, China

8 ²Institute of Land Surface System and Sustainable Development, Faculty of Geographical Science,
9 Beijing Normal University, Beijing, China

10 ³Institute of Carbon Neutrality, Laboratory for Earth Surface Processes, College of Urban and
11 Environmental Sciences, Peking University, Beijing 100871, China

12 ⁴State Key Laboratory of Regional and Urban Ecology, Research Center for Eco-Environmental
13 Sciences, Chinese Academy of Sciences, Beijing 100085, China

14

15 **Corresponding Author:**

16 Yan Li, Ph.D.

17 Institute of Land Surface System and Sustainable Development, Faculty of Geographical Science,
18 Beijing Normal University, Beijing, 100875, China

19 Email: yanli.geo@gmail.com

20

21 **Abstract:** Modeling the coupled human–natural systems (CHANS) is vital for
22 understanding human–natural interactions and achieving regional sustainability,
23 offering a powerful tool to alleviating human–water conflicts, ensuring food security,
24 thereby supporting the region’s pathway toward sustainable development. However, the
25 scarcity of regional-scale CHANS models constrains progress in practical applications
26 for regional sustainability. The Yellow River basin (YRB) is an ideal region for

27 modeling regional CHANS due to its closely coupled human and natural systems,
28 which are stressed by water and ecosystem fragility. Here, we developed the CHANS-
29 SD-YRB model using the System Dynamics approach, integrating 10 sectors essential
30 for modeling human-water interactions of the basin, including five human sectors
31 (Population, Economy, Energy, Food, and Water Demand) and five natural sectors
32 (Water Supply, Sediment, Land, Carbon, and Climate). The model can simulate
33 evolution and feedbacks of the YRB CHANS annually at provincial and sub-basin
34 scales, while conserving hydrological connectivity between sub-basins. The model can
35 accurately reproduce historical CHANS dynamics, achieving strong quantitative
36 agreement with historical data ($R > 0.95$ for human sectors and $R > 0.7$ for natural
37 sectors), which supports its applicability for scenario analyses and future projections.
38 We applied the model to explore human–natural system dynamics under a future
39 baseline scenario, assuming the continuation of existing policies and climate projection
40 under middle of the road scenario (SSP–RCP 2-4.5). The future projections (2021-2100)
41 indicate that achieving sustainable development in the YRB will remain challenging,
42 though economic growth and food security are expected to improve. Emerging issues,
43 such as ecological–human water trade-offs, labor shortages, reduced sediment load, and
44 limited carbon absorption capacity, may hinder regional long-term sustainability.

45 **Keywords:** coupled human-natural systems, regional modeling, system dynamics,
46 the Yellow River Basin

47 **1 Introduction**

48 Coupled human and natural systems (CHANS) emphasize the reciprocal feedback
49 and co-evolution between human and natural systems, offering an integrated framework
50 for diagnosing complex problems and guiding sustainable development (Fu and Li,
51 2016). By capturing dynamic interactions of interconnected components, CHANS
52 theories and models enable more effective policies and interventions that align
53 ecological integrity with socioeconomic progress (Motesharrei et al., 2016; Verburg et
54 al., 2016). Numerous integrated modelling approaches have been developed to simulate

55 human–natural interactions at the global scale. These include system dynamics-based
56 integrated assessment models (IAMs), such as ANEMI (Breach and Simonovic, 2021),
57 FeliX (Rydzak et al., 2013; Ye et al., 2024), and FRIDA (Rajah et al., 2025), process-
58 based and optimization-based IAMs (Vaidyanathan, 2021), and Earth system models
59 with synchronously coupled human components, such as E3SM-GCAM (Di Vittorio et
60 al., 2025) and integrated Earth system models (iESMs) (Jain et al., 2022). These models
61 effectively characterize human–natural interactions at the global scale, and have been
62 applied to assess the impacts of climate change on human society (e.g., agriculture
63 (Monier et al., 2018), economic damage (Wang et al., 2020b), fatalities increase and
64 welfare loss (Dottori et al., 2018)), and humans’ feedback on the Earth system, such as
65 those from climate mitigation on water and food security (Cheng et al., 2022; Fujimori
66 et al., 2022).

67 Currently, most CHANS models are at the global scale (Calvin and Bond-
68 Lamberty, 2018) with much fewer regional models. While global modeling research
69 has deepened our knowledge of dynamic feedbacks among Earth’s spheres and system
70 evolution under climate change, sustainability challenges often manifest at regional
71 scales, where social and ecological dynamics are more intricately intertwined (Liu et
72 al., 2007). Compared to global CHANS, regional CHANS are open systems that
73 continuously exchange energy and materials with other regions and the global system,
74 e.g., water resources and electricity transfers (Dobbs et al., 2023; Zhang et al., 2022a)
75 and trade (Ristaino et al., 2021), resulting in pericoupling and telecoupling of different
76 systems (Liu, 2017). Besides, regional CHANS are shaped by more immediate and
77 complex human influences and stressors, such as urban expansion (van Vliet, 2019),
78 ecological protection (Xu et al., 2017; Yang et al., 2022), and water resource regulation
79 policies (diversion and allocation) (Song et al., 2024), which alter regional CHANS
80 dynamics. Due to their diverse ecological and socioeconomic resilience, regional
81 CHANS exhibit heterogeneous responses to external weather events and climate
82 change, as evidenced by differing responses in crop yield (Hasegawa et al., 2021) and

83 economic production to extreme heat and warming (Waidelich et al., 2024a).
84 Furthermore, the coarse spatiotemporal resolution of global models limits their capacity
85 to support effective decision-making for regional development (X. Li et al., 2018). As
86 such, advancing regional CHANS modeling is essential for informing adaptive
87 strategies in the face of growing regional environmental and societal pressures.

88 To address this limitation, many regional CHANS models have been developed at
89 various regional scales (e.g., national, basin, and urban) using System Dynamics (SD)
90 and agent-based modeling (ABMs) techniques. Notable examples include the ANIME-
91 Yangtze model (Jiang et al., 2022), the T21-China (Qu et al., 2020), and the iSDG-
92 Australia model (Allen et al., 2019), all based on SD, the Jordan Water Model (Yoon et
93 al., 2021) with its core on ABM, as well as integrated models in the San Juan River
94 Basin (Hyun et al., 2019) and the Heihe River Basin (Li et al., 2021). These models are
95 designed to capture finer-scale dynamics and region-specific human–natural
96 interactions, since they embed localized characteristics (e.g., fishing ban, reservoir
97 operation strategies, demographic policies, transboundary flows) and account for
98 heterogeneity overlooked by global models. As a result, regional CHANS models offer
99 stronger policy relevance, providing actionable insights for national, basin, and urban
100 decision-making, and advancing CHANS research across multiple scales.

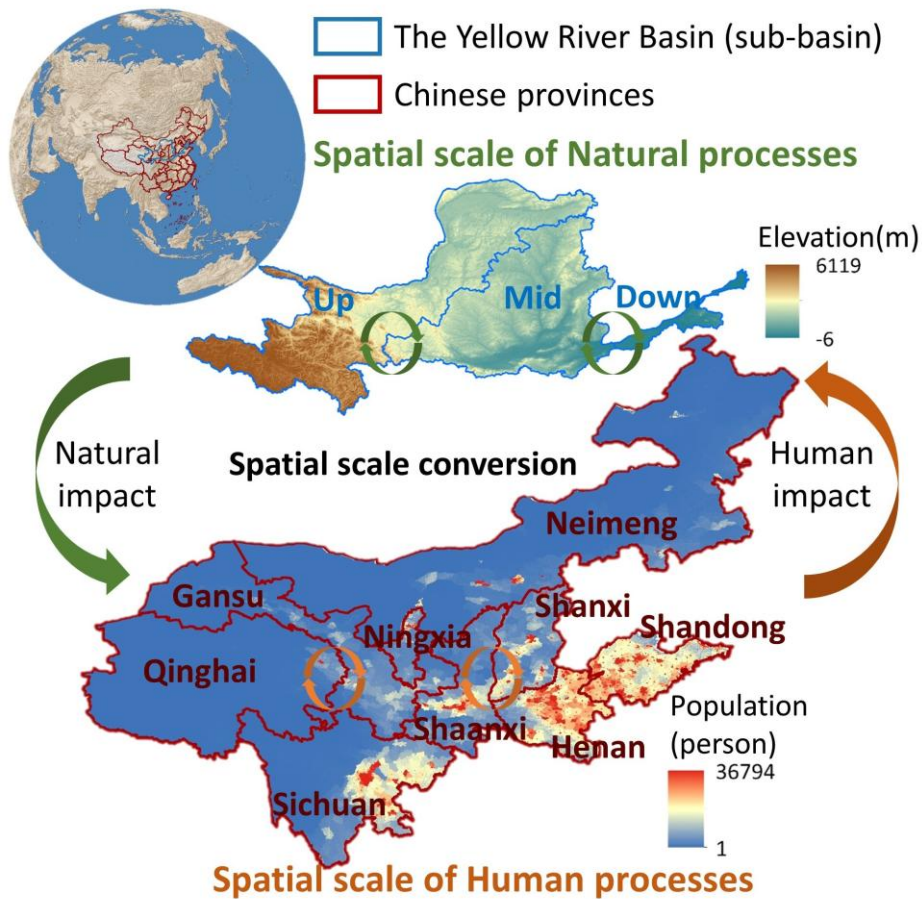
101 The Yellow River Basin (YRB) in China is one of the regions where conflicts
102 between human and natural systems are most acute and complex, particularly in terms
103 of human–water relations, due to the severe imbalance between socioeconomic
104 development and natural hydrological, ecosystem processes. The YRB faces severe
105 water stress, with the water resource utilization rate exceeding 80% (Feng and Zhu,
106 2022; Zhang et al., 2022b). Intensive water extraction has triggered a series of
107 ecological and environmental issues, including flow interruptions, water pollution, and
108 declining groundwater levels, all of which in turn constrain socioeconomic
109 development. The Yellow River traverses the Loess Plateau (Zhu et al., 2019), where
110 severe soil erosion makes the Yellow River one of the most sediment-laden rivers

111 globally (Fu et al., 2011; Yin et al., 2021). The pronounced spatial and temporal
112 variability in streamflow and sediment load leads to significant riverbed aggradation,
113 frequent flooding, and disruption of agricultural production and other livelihood
114 activities (Miao et al., 2016). Due to internal hydrological connectivity, sub-basins are
115 highly interconnected and are susceptible to upstream influences. Upstream water
116 overuse diminishes downstream availability (Wei et al., 2023), a factor that played a
117 major role in flow interruptions during the 1990s (Changming and Shifeng, 2002; Wang
118 et al., 2019). Ecological challenges differ across the subbasin, with the upstream facing
119 ecosystem degradation and limited water retention (Ning et al., 2022), the midstream
120 characterized by soil erosion and large-scale ecological restoration (Fu et al., 2011), and
121 the downstream focusing on wetland conservation (Fu et al., 2023). Policy measures
122 aimed at ecological restoration, such as afforestation and cropland conversion, have
123 increased vegetation cover, reduced sediment loads but also decreased runoff,
124 exacerbating water scarcity (Feng et al., 2016; Wang et al., 2016). These interlinked
125 dynamics underscore the YRB as a complex coupled human–natural system, where
126 addressing environmental challenges requires an integrated, systems-oriented approach.

127 The existing models for the YRB are typically designed for specific problems with
128 a narrow application focus and only represent a limited set of human and natural
129 components within the CHANS. These include limited nature-to-human impact
130 pathways, e.g., low flows threatening farmers’ livelihoods (Liu et al., 2008), the damage
131 of floods and droughts on agriculture (Zhang et al., 2015), as well as human-to-nature
132 impact pathways, e.g., effects of ecological restoration policy on hydropower and
133 water–sediment–carbon dynamics (Wu et al., 2025; Yan et al., 2024), and the impacts
134 of irrigation water-saving and salinity-control practices on crop yield and water
135 productivity (Wu et al., 2023). These models focus on isolated components of CHANS,
136 with limited consideration of fully coupled human–natural interactions, which limits
137 their capacity to represent full human–natural interactions and support regional
138 decision-making.

139 To address the gap in CHANS modeling for the YRB, following our previously
 140 proposed CHANS modeling framework for the basin (Sang et al., 2025b), we
 141 implemented the framework to develop the coupled human and natural systems model
 142 for the YRB (CHANS-SD-YRB) using the System Dynamics approach. Through
 143 dynamic interaction with policies, climate change, human activities, and environmental
 144 feedbacks, the CHANS-SD-YRB model provides a platform for predicting system
 145 dynamics, conducting scenario analyses, evaluating policies, and optimizing water-
 146 food-carbon synergies. This study presents a detailed description and methodological
 147 documentation of the model, offering both theoretical and practical insights to advance
 148 regional CHANS modeling and promote sustainable development in the YRB.

149 **2 Description of the CHANS-SD-YRB**



150

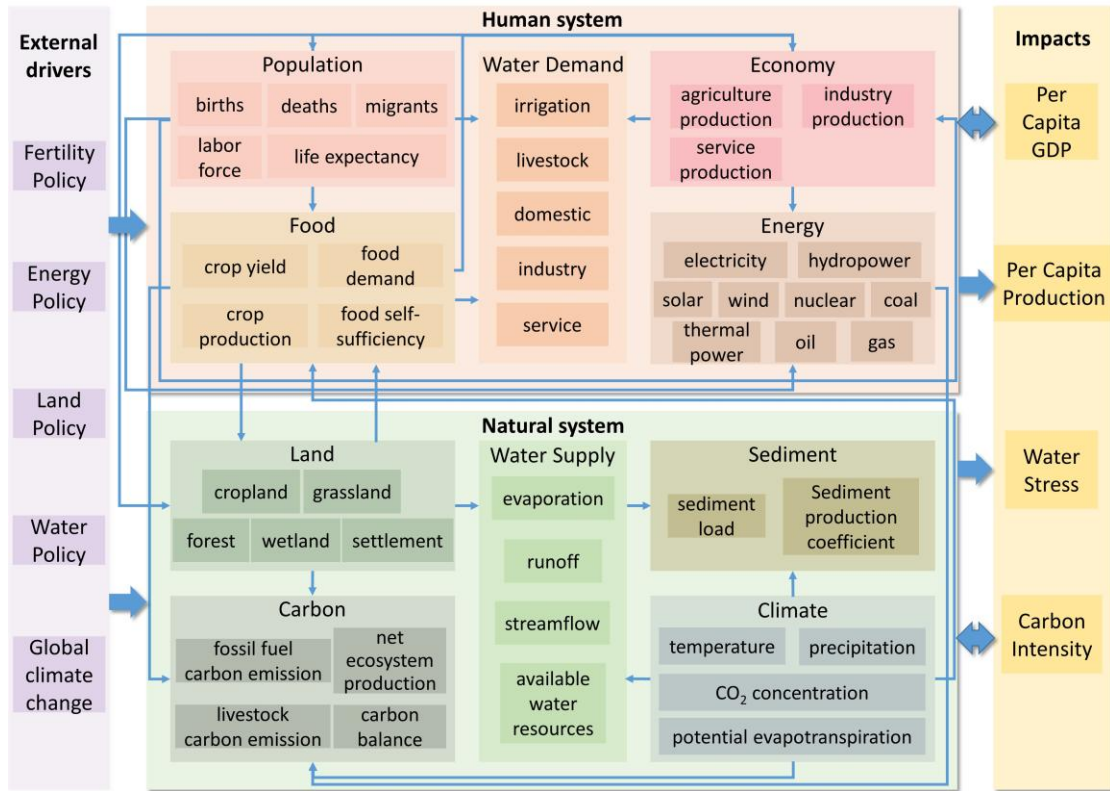
151 Fig.1 Geolocation of the Yellow River Basin and boundary of the natural and human

152 processes in the CHANS-SD-YRB model. Natural processes are simulated at the sub-

153 basin scale (base map: elevation), and human processes at the provincial scale across
154 nine provinces (base map: population density in 2020).

155 We developed the CHANS-SD-YRB based on system dynamics, a method well-
156 suited for capturing complex system behaviors characterized by nonlinearity, multi-
157 level structures, and feedback loops (Forrester, 1968; Richardson, 2011). The model
158 was constructed and implemented using the VENSIM DSS (Ventana Systems, 2023)
159 software platform, operating on an annual time step. The CHANS-SD-YRB simulates
160 both human and natural processes for historical simulations (1981–2020) and future
161 projections (2021–2100). Human processes are simulated at the provincial scale,
162 covering the nine provinces along the Yellow River (Qinghai, Sichuan, Gansu, Ningxia,
163 Neimeng, Shaanxi, Shanxi, Henan, and Shandong), while natural processes are
164 simulated at the sub-basin scale (up-, mid-, and downstream) (Fig.1). The model is
165 designed to capture the various interactions within and between different components
166 of human system and natural system across administrative and hydrological units. The
167 spatial scale conversion between provincial and sub-basin levels relies on weights (e.g.,
168 the proportion of sub-basin-level values to provincial total values) derived from
169 historical high-resolution gridded datasets of human-related variables. These weights
170 enable disaggregation of provincial outputs to the sub-basin level (see Supporting
171 Information S4 for details). Given the availability of gridded data for human processes
172 and the strong correlations among relevant variables, gridded population and GDP data
173 were used as proxies to disaggregate demographic variables and economic and human
174 carbon emissions, respectively, from provincial-level to the sub-basin scale (Table S3).

175 **2.1 Model structure**



176

177 Fig.2 Structure of the CHANS-SD-YRB, which shows sectors of human and natural
 178 systems, their key processes and interactions.

179 Drawing on the modeling framework of CHANS in the YRB (Sang et al., 2025b),
 180 we designed the CHANS-SD-YRB structure (Fig. 2), including five sectors related to
 181 human society (*Population, Economy, Energy, Food, and Water Demand*), and five
 182 sectors related to natural ecosystem (*Water Supply, Sediment, Land, Carbon, and*
 183 *Climate*).

184 These sectors are interconnected to represent various human-natural interactions
 185 as summarized below. Key interactions among human system modules are summarized
 186 below. The *Population* sector affects food demand (*Food*), residential water use (*Water*
 187 *Demand*), household electricity and gas consumption (*Energy*), and settlement land area
 188 (*Land*). The sector also interacts dynamically with the *Economy* sector, where economic
 189 output influences deaths and migrants, while the labor force, in turn, drives economic
 190 production. The *Economy* sector drives energy uses (electricity, coal, oil, and gas use)

191 from *Energy*, as well as industrial and service water withdrawal from *Water Demand*.
192 The gross agricultural production in the *Economy* is made up of crop and livestock
193 production (*Food*). The *Energy* sector produces fossil fuel emissions in the *Carbon*
194 sector. The *Food* sector is affected by the *Land* and *Climate* sector, and it also
195 determines irrigation water withdrawal (*Water Demand*) and livestock-related
196 emissions (*Carbon*). Additionally, the *Food* sector interacts closely with the *Land* sector,
197 where crop production depends on cropland area, which, in turn, is influenced by food
198 self-sufficiency. The *Water Demand* sector affects streamflow in the *Water Supply*
199 sector through consumptive water use.

200 The key interactions among natural system modules are listed below. The *Land*
201 sector influences evapotranspiration in the *Water Supply* sector through vegetation
202 coverage, and it influences carbon absorption in *Carbon* sector through land use area.
203 The carbon absorption is also affected by climatic variables including temperature,
204 precipitation, and CO₂ concentration. Similarly, runoff in the *Water Supply* sector is
205 affected by precipitation, precipitation intensity (mm/h, the rate of rainfall within one
206 hour calculated from daily data), and potential evapotranspiration. Streamflow
207 influences sediment dynamics in the *Sediment* sector together with the *Climate* sector.

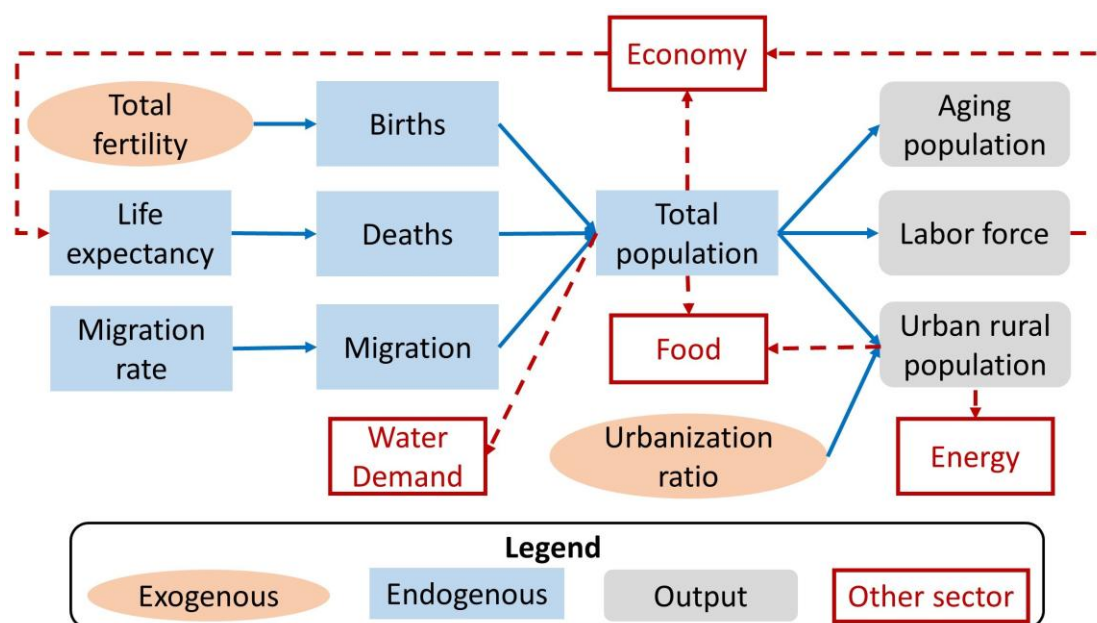
208 In addition, the CHANS dynamics in the YRB are modulated by external drivers,
209 including policies and global climate change that affect various modeled processes (e.g.,
210 fertility, energy, land use, and water). With comprehensive representation of CHANS
211 processes and their interactions, the CHANS-SD-YRB model is capable of generating
212 integrated indicators to assess the state of the coupled system, such as per capita GDP,
213 per capita food production, water stress, and carbon intensity. These indicators not only
214 serve as evaluation metrics but also feed back to influence the internal dynamics of the
215 human–natural system in the YRB.

216 **2.2 Sector description**

217 The CHANS-SD-YRB model focuses on the essential human–natural processes in
218 the YRB, with a particular emphasis on human–water interactions. To this end, it has a

219 comprehensive representation of the full range of natural and human processes that
 220 influence water use and supply. Formulation of each sector aims to explicitly account
 221 for cross-sectoral interactions as fully as possible while remaining sufficiently simple
 222 to be implemented within the SD software. Considering data availability and the spatial
 223 scales of process, human sectors (*Population, Economy, Energy, Food, and Water*
 224 *Demand*) are simulated at the provincial level, while natural sectors (*Water Supply,*
 225 *Sediment, Land, Carbon, and Climate*) are simulated at the sub-basin level within the
 226 YRB. Next, we describe each sector and its key formulation and provide full details in
 227 Supporting Information S2.

228 2.2.1 Population



229
 230 Fig.3 Structure of the *Population* sector. Blue lines indicate connections inside the
 231 sector, red dotted lines indicate connections with other sectors.

232 Population dynamics are driven by births, deaths, and migration (Fig. 3). Births
 233 are calculated based on exogenous total fertility rates derived from historical data
 234 (Equation S2) to reflect the strong influence of China's Family Planning Policy. Deaths
 235 are determined by the life expectancy, which is modeled as a function of human well-
 236 being (Equations S3-S6). Migration is calculated based on historical statistical data and
 237 per capita GDP differences between YRB and the national average level (Equations S7-

238 S8). The total population is characterized by age and gender with exogenous
 239 urbanization ratios. The output of *Population* sector drives *Economy*, *Energy*, *Food*,
 240 and *Water Demand* sectors through labor force, urban and rural populations.

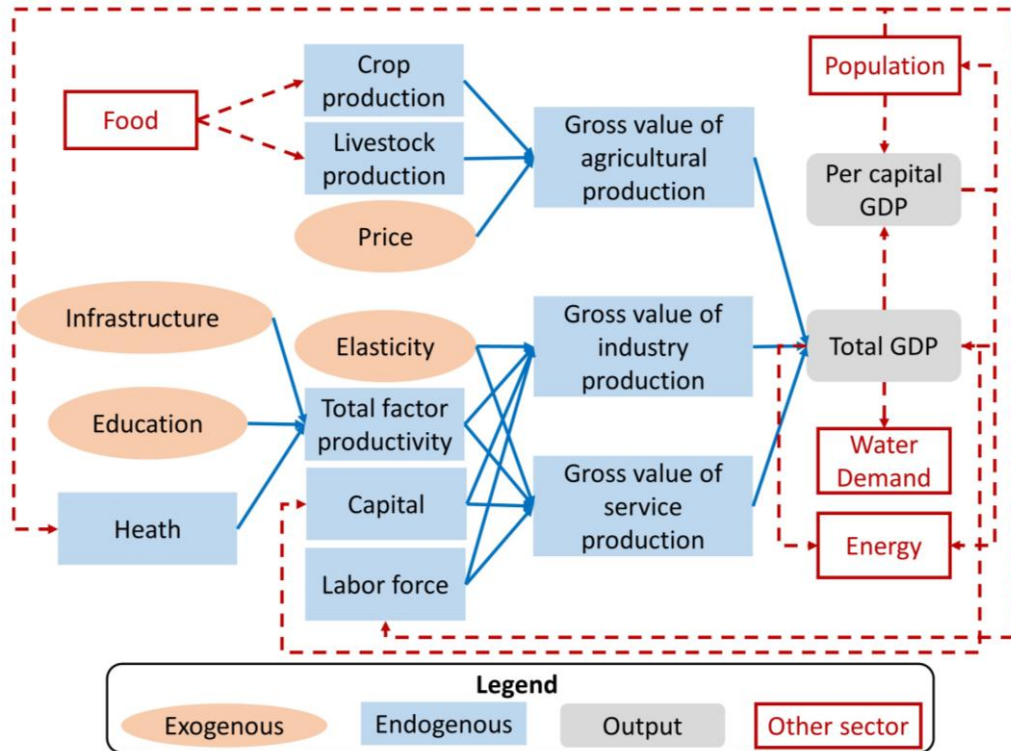
241 The key variable, total population, is modeled using the age-structured
 242 mathematical method (Kemei et al., 2024), which categorizes individuals by one-year
 243 age group and gender (Equation 1),

$$244 \text{Pop}_{g,a} = \text{IniPop}_{g,a} + \begin{cases} \int (B_{g,a} + NM_{g,a} - D_{g,a})dt, & a = 0 \\ \int (\text{Pop}_{g,a} + NM_{g,a} - D_{g,a})dt, & 1 \leq a \leq 99, a = 100 \text{ and over} \end{cases}$$

245 (1)

246 where *Pop* is population, subscript *g* and *a* are gender (*g* = M is male, *g* = F is female)
 247 and age (*a* = 0-100 and over); *IniPop_{g,a}* is the population in the initial year, *B_{g,a}* is the
 248 births, *D_{g,a}* is the deaths, and *NM_{g,a}* is the net migrants (i.e., immigrants – emigrations).

249 **2.2.2 Economy**



250
 251 Fig.4 Structure of the *Economy* sector. Blue lines indicate connections inside the
 252 sector, red dotted lines indicate connections with other sectors.

253 The *Economy* sector simulates production activities in agriculture, industry, and

254 services, which in turn drive changes in the *Population, Energy, and Water Demand*
255 sectors (Fig. 4).

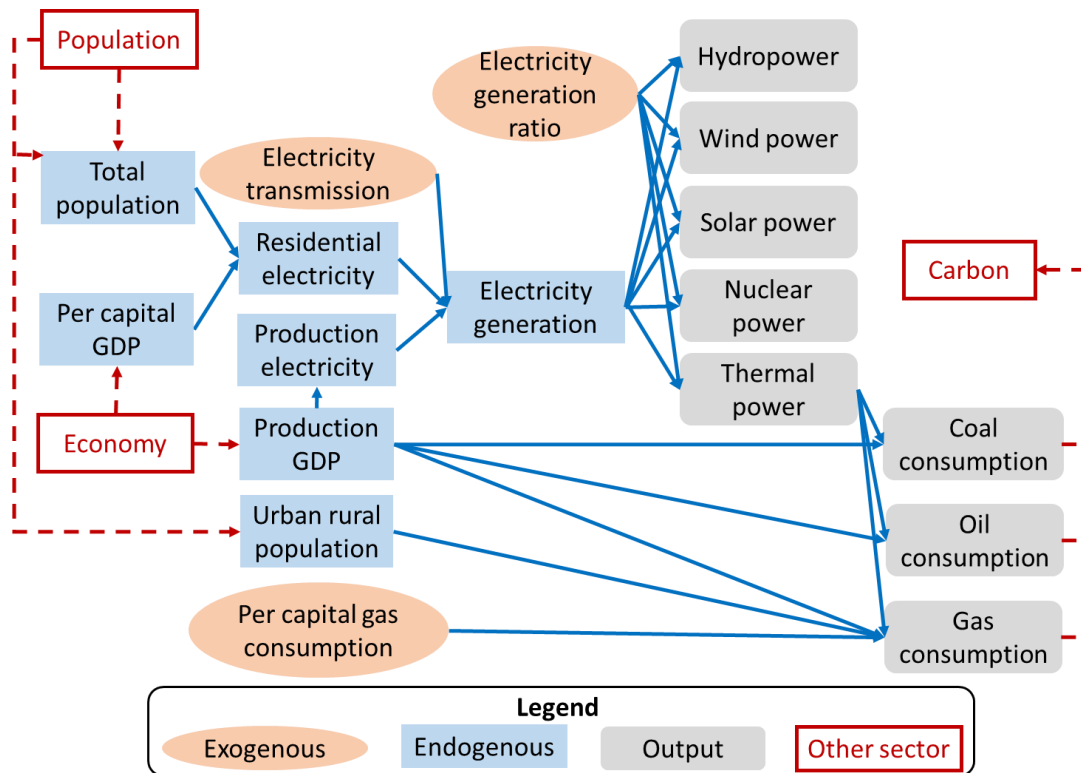
256 The gross product of industry and services is calculated using the Cobb-Douglas
257 production function (Cobb and Douglas, 1928) to account for multiple factors in the
258 economy (Equation 2). Exogenous variables (infrastructure, education, and elasticity),
259 and endogenous variables (health and labor force) from the *Population* sector
260 (Equations S10-S21) all affect the gross domestic product in industry and service
261 (GDP_s),

$$262 \quad GDP_s = IniGDP_s \times TFP_s \times \left(\frac{L_s}{IniL_s}\right)^{1-\alpha_s} \times \left(\frac{K_s}{IniK_s}\right)^{\alpha_s} \quad (2)$$

263 where subscript s represents industry and service, $IniGDP_s$ is the initial GDP; TFP_s is
264 the total factor productivity calculated from exogenous (infrastructure, education, and
265 elasticity) and endogenous variables (health and labor force) (Equations S10-S13); L_s
266 represents the labor force and $IniL_s$ is its initial value (from *Population* sector); α_s and
267 $1-\alpha_s$ are capital and labor elasticities from T21-China (Qu et al., 2020) and calibrated
268 using historical data; K_s and $IniK_s$ refer to the capital stock and its initial level.

269 Gross agricultural production includes crop and livestock production from *Food*
270 sector, calculated by their respective prices (Equations S22-S23).

271 **2.2.3 Energy**

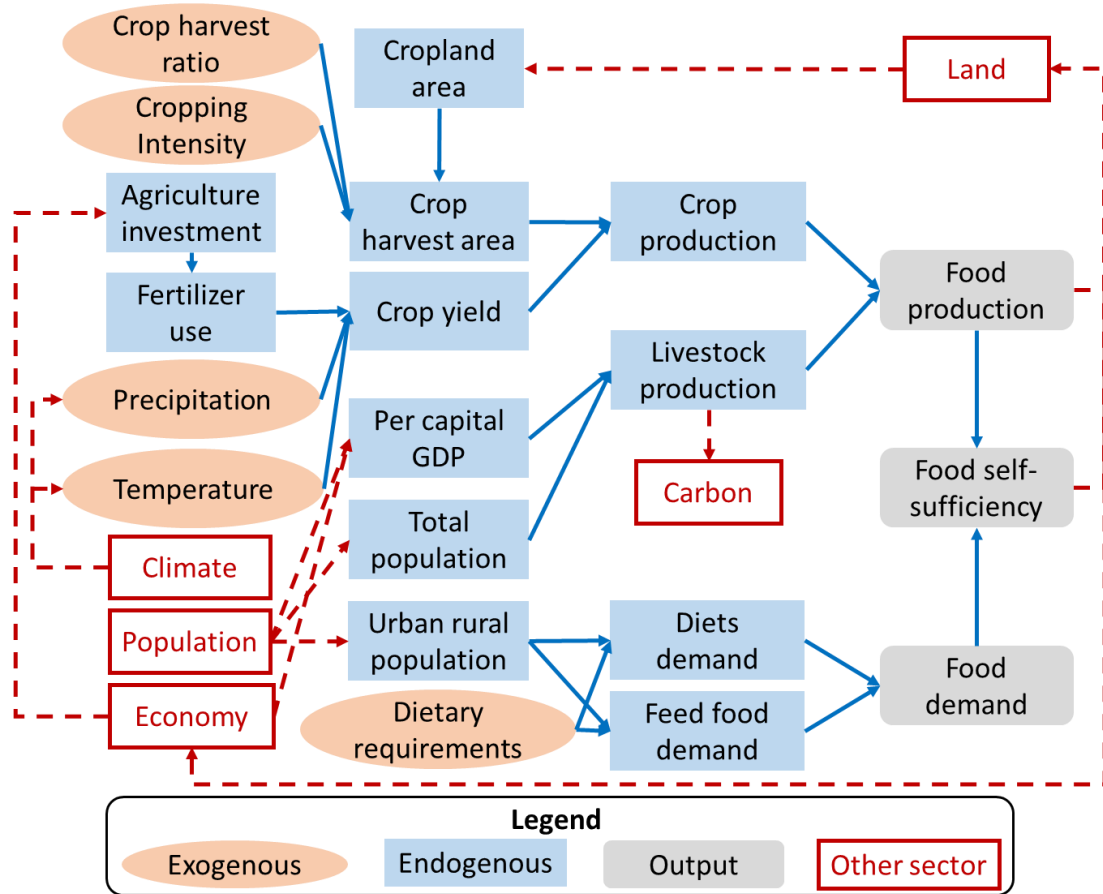


272
 273 Fig.5 Structure of the *Energy* sector. Blue lines indicate connections inside the sector,
 274 red dotted lines indicate connections with other sectors.

275 The *Energy* sector simulates production, consumption, and the structure of the
 276 energy system, encompassing fossil fuels (coal, oil, and gas) and electricity (Fig. 5).
 277 Energy production and consumption are always balanced in this sector. Electricity
 278 generation is divided into residential and production uses, the former is estimated from
 279 the linear fit of historical per capita GDP and residential demand, and the latter is
 280 calculated using GDP and electricity intensity data from the China Energy Statistical
 281 Yearbook (NBSC, 2020a) (Equations S24-S25). Cross-provincial electricity
 282 transmission is also incorporated according to the same yearbook. The shares of
 283 electricity generated from thermal, hydro, wind, solar, and nuclear sources are
 284 determined by exogenously specified ratios, as reported in the China Energy Statistical
 285 Yearbook (NBSC, 2020a). The fossil fuel consumption by economic production of
 286 industry and service sectors is modeled as a linear function of sectoral GDP based on
 287 historical data (Equations S26-S28). It combines with fossil fuel consumption for

288 electricity generation and residential gas consumption to drive carbon emissions in the
 289 *Carbon* sector.

290 **2.2.4 Food**



291
 292 Fig.6 Structure of the *Food* sector. Blue lines indicate connections inside the sector,
 293 red dotted lines indicate connections with other sectors.

294 The *Food* sector simulates the production of livestock and crops, and food demand,
 295 and these productions directly affect gross agricultural production in the *Economy*
 296 sector (Fig. 6). Livestock production ($Livestock_{pro}$) is calculated by an empirical
 297 function, driven by economic development and population growth (Equation 3),

298
$$Livestock_{pro} = Pop \times \left(Para_{GL1} + (Para_{GL2} - Para_{GL1}) \times \frac{PCGDP}{PCGDP + ConstGL} \right) \quad (3)$$

299 where $Para_{GL1}$, $Para_{GL2}$ and $ConstGL$ are parameters obtained by fitting the historical
 300 per capita meat production and per capita GDP ($PCGDP$) data.

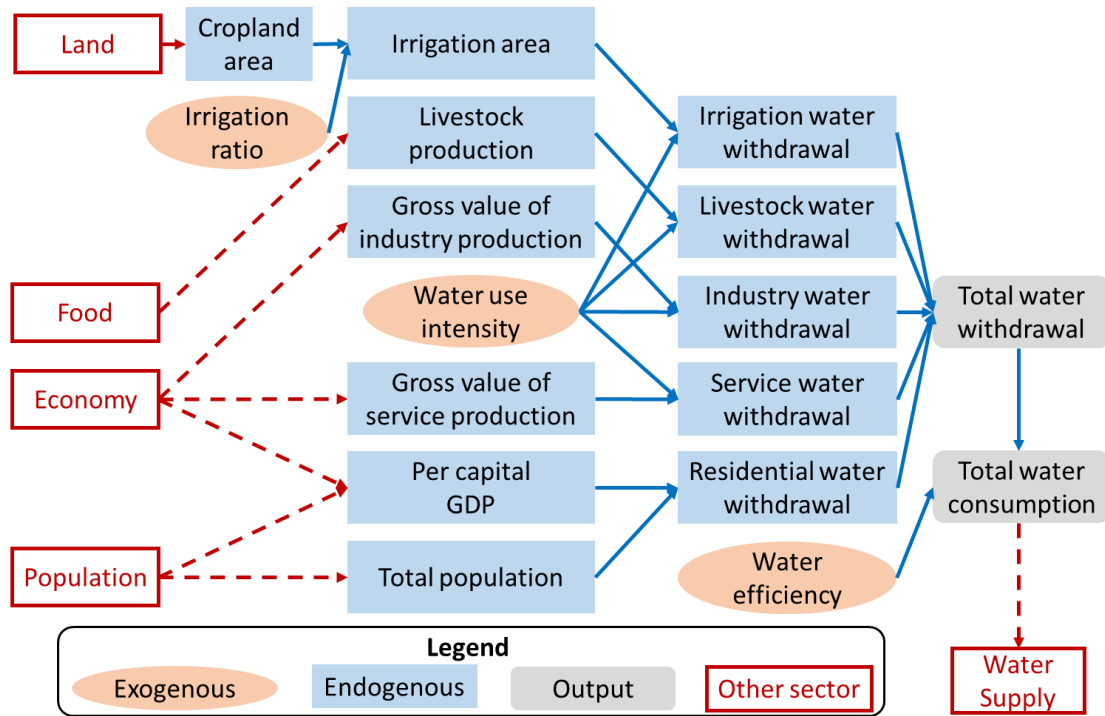
301 Crop production ($Crop_{pro}$) is determined by the yield ($Yield_c$) and harvest area (PA_c)
 302 of seven major crop types (subscript c): rice, wheat, corn, soybeans, cotton, potatoes,

303 and oil crops (Equation 4). The harvest area is influenced by cropland area from the
 304 *Land* sector, exogenous cropping intensity and crop harvest ratio. Crop yields are
 305 positively affected by agricultural investment from the *Economy* sector, along with
 306 effects of precipitation, temperature, and CO₂ concentration from the *Climate* sector
 307 (Equations S30-S36).

308
$$Crop_{pro} = \sum_{c=1}^7 Yield_c \times PA_c \quad (4)$$

309 Food demand encompasses both staple and feed grain demand, which are
 310 determined by population size from *Population* sector and dietary patterns (Equations
 311 S37-S41).

312 **2.2.5 Water Demand**



313
 314 Fig.7 Structure of the *Water Demand* sector. Blue lines indicate connections inside the
 315 sector, red dotted lines indicate connections with other sectors.

316 The *Water Demand* sector simulates water withdrawal (*WW*) and consumption
 317 (*WC*) across multiple uses—irrigation, livestock, industry, services, and residential—
 318 in the nine provinces of the YRB (Fig. 7). Water consumption is derived as the product
 319 of water withdrawal and water use efficiency reported in the Water Resources Bulletin
 320 (YRCCMWR, 2020) (Equations S42-S43), which affects the *Water Supply* sector.

321 Irrigation water withdrawal (WW_{irr}) is estimated through a physically-based
 322 function of exogenous irrigation water use intensity (WWI_{irr}), cropland irrigation ratios
 323 (IR) from the China Agricultural Yearbook (MAARA, 2020), and cropland area
 324 ($Area_{Cropland}$) provided by the *Land* sector (Equation 5).

$$325 \quad WW_{irr} = WWI_{irr} \times Area_{Cropland} \times IR \quad (5)$$

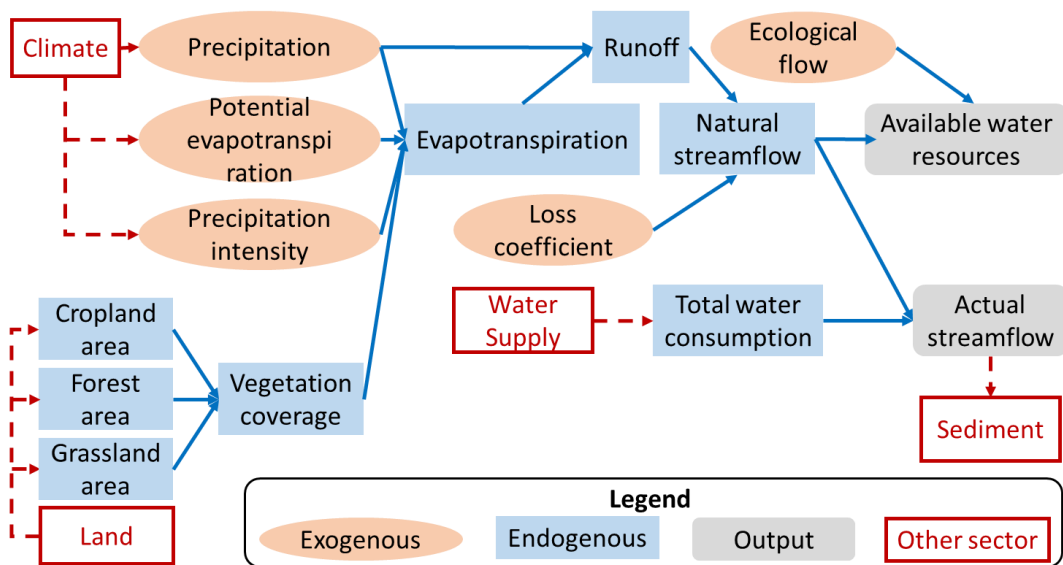
326 The water withdrawal for livestock, industry, and services is also driven by
 327 exogenous sectoral water use intensities collected from the China Statistical Yearbook
 328 and National Long-term Water Use Dataset of China (Zhou et al., 2020), in combination
 329 with livestock production from the *Food* sector, economic output from the *Economy*
 330 sector (Equations S45-S48).

331 Residential water withdrawal (WW_{res}) is derived from a non-linear empirical
 332 function of economic development and population growth with an upper limit of per
 333 capita domestic water use (Flörke et al., 2013) because water demand per person cannot
 334 increase indefinitely (Equation 6),

$$335 \quad WW_{res} = Pop \times \left(Para_{GD1} + (Para_{GD2} - Para_{GD1}) \times \frac{PC_{GDP}}{PC_{GDP} + Const_{GD}} \right) \quad (6)$$

336 where $Para_{GD1}$, $Para_{GD2}$, and $Const_{GD}$ are parameters obtained by fitting the historical
 337 per capita domestic water use with per capita GDP (PC_{GDP}).

338 2.2.6 Water Supply



339

340 Fig.8 Structure of the *Water Supply* sector. Blue lines indicate connections inside the
 341 sector, red dotted lines indicate connections with other sectors.

342 The *Water Supply* sector simulates runoff, discharge, and their changes in each
 343 sub-basin (Fig. 8). Runoff (R) is determined by precipitation (Pre) and
 344 evapotranspiration (ET) based on the water balance principle derived from the Budyko
 345 equation, which is suitable for non-humid regions of China (Yang et al., 2009)
 346 (Equation 7).

$$347 \quad R = Pre - ET \quad (7)$$

348 The ET is calculated by various exogenous climate variables from the *Climate*
 349 sector, and vegetation coverage from the *Land* sector (Equations 8-9, S51-S53),

$$350 \quad ET = \frac{PET \times Pre}{(Pre^n + EP^n)^{\frac{1}{n}}} \quad (8)$$

$$351 \quad n = Para_{E1} \times \left(\frac{KS}{PI}\right)^{Para_{E2}} \times FVC^{Para_{E3}} \times e^{Para_{E4} \tan \beta} \quad (9)$$

352 where PET is potential evapotranspiration at sub-basin, from the *Climate* sector; n is a
 353 parameter reflecting the basin landscape characteristics, related to saturated hydraulic
 354 conductivity (KS), precipitation intensity (PI), average slope (β), and fraction of
 355 vegetation coverage (FVC); $Para_{E1}$, $Para_{E2}$, $Para_{E3}$, and $Para_{E4}$ are parameters fitted
 356 from historical data.

357 Runoff and the loss coefficient (defined by the ratio of natural streamflow to runoff)
 358 determine the natural streamflow due to the water loss during the confluence process
 359 (Equation S54). Natural streamflow and ecological flow constraints define the upper
 360 limit of available water resources. By integrating human water consumption from the
 361 *Water Demand* sector across sub-basins, the model calculates the actual streamflow
 362 (Equations S55-S57). Actual streamflow is transferred through hydrological
 363 connectivity from upstream to midstream and then to downstream, ultimately reaching
 364 the sea, which governs sediment transport processes within the *Sediment* sector.

365 **2.2.7 Sediment**

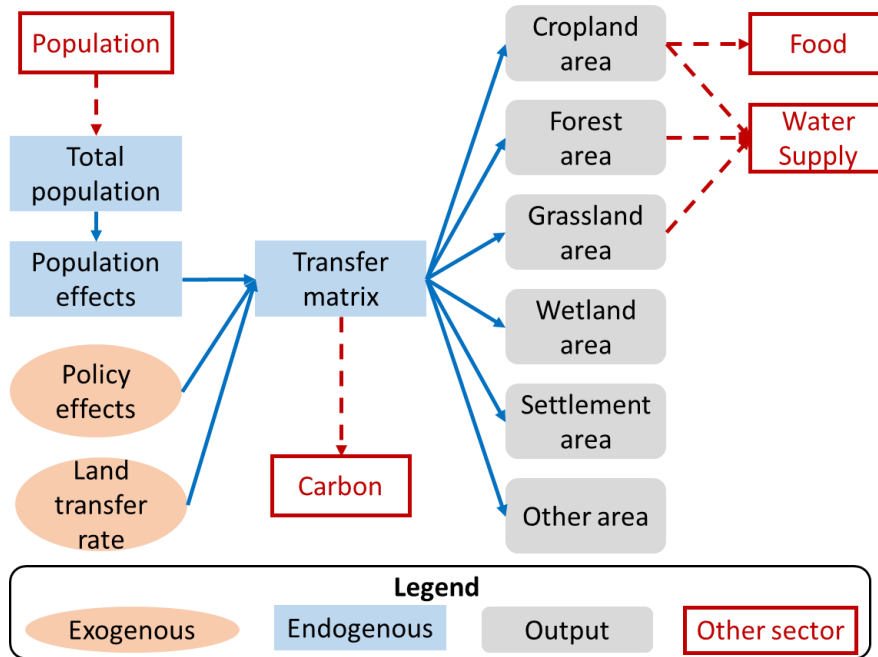
366 The *Sediment* sector estimates sediment load (Sed) for each sub-basin using an

367 empirical model in the literature (Yin et al., 2023b), which links actual streamflow from
 368 the *Water Supply* sector to sediment transport,

369
$$Sed = Para_{SS} \times AS + Const_{SS} \quad (10)$$

370 where *Parass* and *Constss* are derived from linear fitting of historical hydrological
 371 station data on actual streamflow and sediment load.

372 **2.2.8 Land**



373

374 Fig.9 Structure of the *Land* sector. Blue lines indicate connections inside the sector,
 375 red dotted lines indicate connections with other sectors.

376 The *Land* sector simulates the area changes of six land use types (cropland, forest,
 377 grassland, wetland, settlement, and others) based on the land transfer matrix obtained
 378 from historical remote sensing data (Xu et al., 2018). The land transfer matrix calculates
 379 the inflow and outflow of each land category and can be configured to represent the
 380 influence of future land use drivers (Fig. 9). This sector outputs vegetation area
 381 (including forest, grassland, and cropland), which influences the *Water Supply* sector.
 382 Cropland area changes impact the *Food* sector, while land use conversion also plays a
 383 role in the *Carbon* sector.

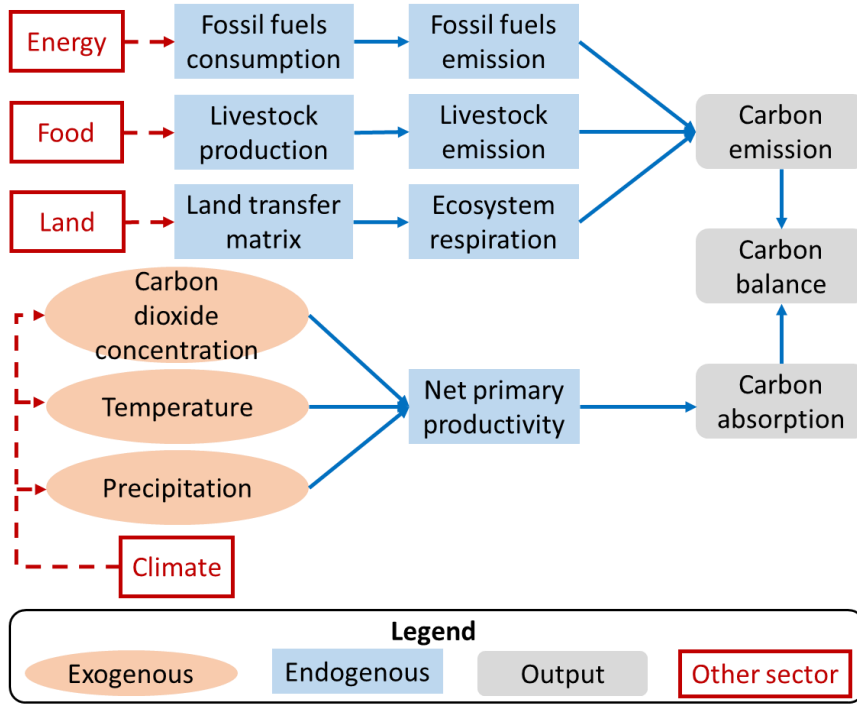
384 Based on the initial land use area (*IniArea_i*), the transfer matrix determines the area

385 ($Area_i$) allocated to each land use type (Equations 11, S60-S66),

386
$$Area_i = IniArea_i + \int (\sum_{i=1}^6 FTM_{i,j} - \sum_{j=1}^6 FTM_{i,j}) dt \quad (11)$$

387 where $FTM_{i,j}$ is the final land use transfer matrix, indicating the area of land use i
 388 transferred to land use j , i and j represent six land use type.

389 **2.2.9 Carbon**



390

391 Fig.10 Structure of the *Carbon* sector. Blue lines indicate connections inside the
 392 sector, red dotted lines indicate connections with other sectors.

393 The *Carbon* sector simulates the basin’s carbon balance processes, including
 394 carbon emission and absorption, adapted from the carbon cycle of ANEMI (Davies and
 395 Simonovic, 2011). Carbon emissions (CE) encompass fossil fuel emissions, and
 396 livestock emission, and ecosystem respiration, which are influenced by outputs from
 397 the *Energy*, *Food*, and *Land* sectors (Fig. 10).

398 Fossil fuel and livestock emissions are calculated based on fossil fuel consumption,
 399 livestock production, and their respective emission coefficients. Ecosystem emissions
 400 include carbon released from burning as well as from the decomposition of biomass,
 401 litter, humus, and charcoal, which are determined by carbon pools’ lifespans,

402 decomposition factor, and respiration coefficients (Equations S67-S93).

403 Carbon absorption (CA) is determined by net primary productivity (NPP) and land
 404 use area. NPP is influenced by climate factors, including CO_2 concentration,
 405 temperature, and precipitation (Equations 12, S63),

$$406 \quad CA = \sum_{i=1}^6 NPP_i \times Area_i \quad (12)$$

407 where i represent land use type, land use area ($Area_i$) from the *Land* sector.

408 2.2.10 Climate

409 The *Climate* sector supplies both historical and projected climate data essential for
 410 the *Water Supply*, *Food*, and *Carbon* sectors. The key climate variables comprise
 411 temperature and precipitation (at the sub-basin and provincial levels), as well as
 412 potential evapotranspiration, precipitation intensity, and CO_2 concentration (at the sub-
 413 basin level). These variables are treated as exogenous inputs, without accounting for
 414 potential feedbacks from human activities or natural system responses on regional
 415 climate patterns.

416 2.3 Data sources

417 In the model, there are more than 100 exogenous variables, some of which are
 418 initial variables that drive the simulation. These exogenous variables are derived either
 419 from historical statistical data or from fitted results based on historical data (Table S2).

420 All data sources required for the model simulation are listed in Table 1.

421 Table 1. Summary of data sources for the YRB model. Updated from Sang et al.
 422 (2025).

Sector	Variables*	Data sources	Spatial and temporal scale	Time range
Population	age-specific population, births, deaths, migrants	<ul style="list-style-type: none"> China Statistical Yearbook (NBSC, 2020c), China Population Census Yearbook (NBSC, 2020b) 	<ul style="list-style-type: none"> provincial, annual 	<ul style="list-style-type: none"> 1981–2023
Economy	GDP, investment, employment	<ul style="list-style-type: none"> China Agricultural Yearbook (MAARA, 2020), 	<ul style="list-style-type: none"> provincial, annual 	<ul style="list-style-type: none"> 1981–2023

		<ul style="list-style-type: none"> China Statistical Yearbook (NBSC, 2020c) 		
Energy	electricity, coal, oil, gas consumption	<ul style="list-style-type: none"> China Energy Statistical Yearbook (NBSC, 2020a) 	<ul style="list-style-type: none"> provincial, annual 	<ul style="list-style-type: none"> 1981–2023
Food	crop production, fertilizer, irrigated area	<ul style="list-style-type: none"> China Agricultural Yearbook (MAARA, 2020) 	<ul style="list-style-type: none"> provincial, annual 	<ul style="list-style-type: none"> 1981–2023
Water demand	Industrial, domestic, irrigation water withdrawal	<ul style="list-style-type: none"> National Long-term Water Use Dataset of China (NLWUD) (Zhou et al., 2020) China Statistical Yearbook (NBSC, 2020c) 	<ul style="list-style-type: none"> prefectural, annual 	<ul style="list-style-type: none"> 1965–2013 1981–2023
Water supply	runoff, streamflow, water stress	<ul style="list-style-type: none"> China Natural Runoff Dataset (CNRD) (Gou et al., 2021), Gauge-based Natural Streamflow Dataset (Miao et al., 2022) Yellow River Water Resources Bulletin (YRCCMWR, 2020) 	<ul style="list-style-type: none"> 0.25° grid, Monthly 0.25° grid, annual provincial, annual 	<ul style="list-style-type: none"> 1961–2018 1961–2018 1998–2022
Sediment	sediment load	<ul style="list-style-type: none"> Yellow River Water Resources Bulletin (YRCCMWR, 2020) 	<ul style="list-style-type: none"> provincial, annual 	<ul style="list-style-type: none"> 1998–2022
Land	cropland, forest, grassland, wetland, settlement	<ul style="list-style-type: none"> China land use remote sensing monitoring dataset (CNLUCC) (Xu et al., 2018) Long-term global land surface satellite fractional vegetation cover product (Jia et al., 2015, 2019) 	<ul style="list-style-type: none"> 1 km grid, annual 	<ul style="list-style-type: none"> 1980, 1990, 1995, 2000, 2005, 2010, 2015, 2020
Carbon	fossil fuel carbon emissions, net primary productivity	<ul style="list-style-type: none"> Carbon Emission Accounts and Datasets (Shan et al., 2018), Global Vegetation 	<ul style="list-style-type: none"> Provincial, annual 5 km grid, 8 day 	<ul style="list-style-type: none"> 1997–2021 1981–2018

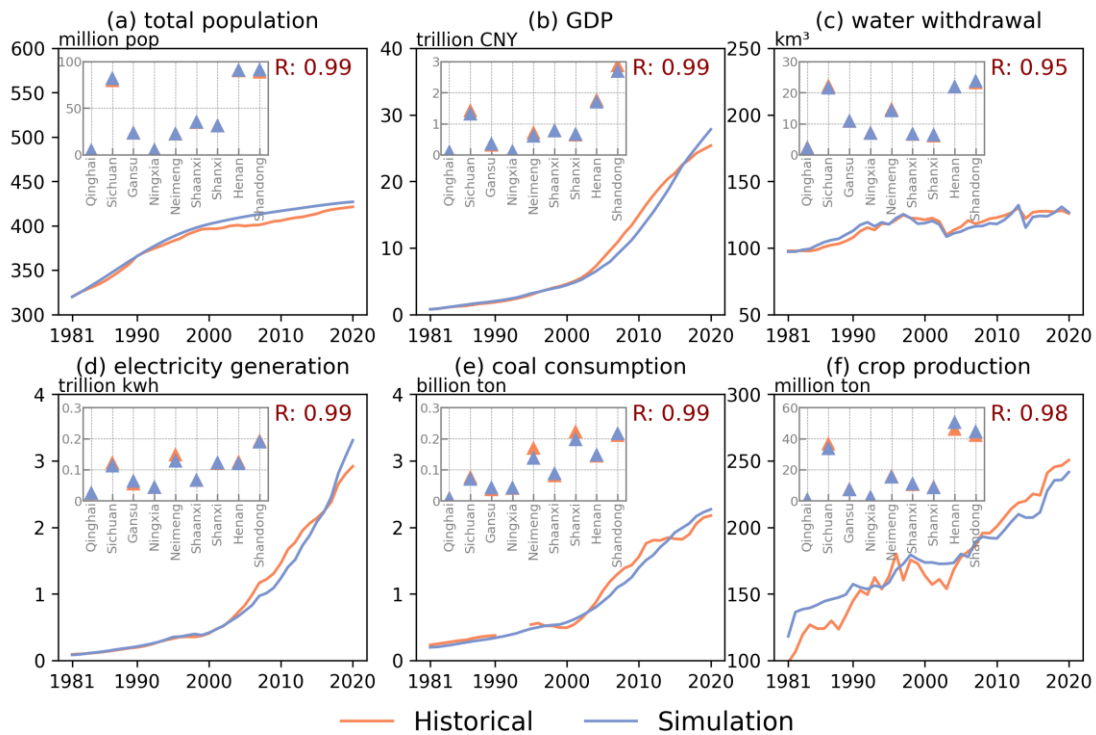
Productivity Products
(GVPP) (Cui et al., 2016;
Wang et al., 2020a; Yu et
al., 2018)

Climate	temperature, precipitation, CO ₂ concentration, potential evapotranspiration and precipitation intensity	<ul style="list-style-type: none"> Gridded daily observation dataset over China region (Wu and Gao, 2013), European Environment Agency (EEA, 2019), China Meteorological Data Service Center (https://data.cma.cn/) 	<ul style="list-style-type: none"> 0.25° grid, Annual Global, Annual Meteorological stations, Monthly 	<ul style="list-style-type: none"> 1961–2020 1800-2020 1956-2018
----------------	--	---	--	---

423 * Listed are some typical variables of each sector

424 **3 Model validation and application**

425 **3.1 Historical model validation**



426

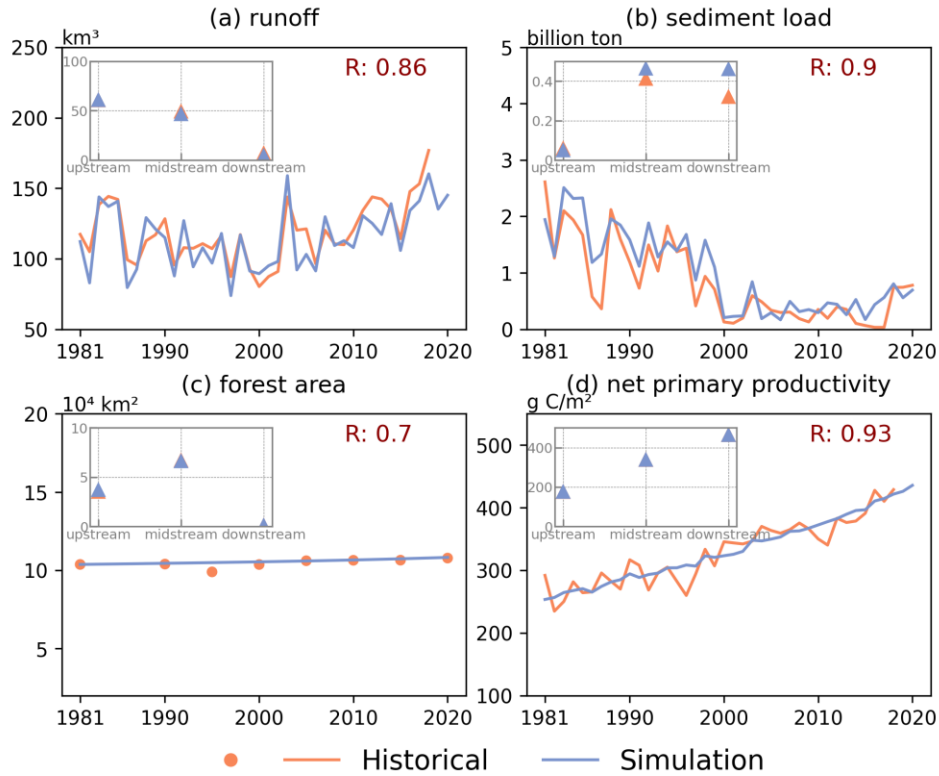
427 Fig.11 Validation of human system processes during historical period of 1981-2020.

428 (a) total population in *Population* sector; (b) GDP in *Economy* sector; (c) water
429 withdrawal in *Water Demand* sector; (d) electricity generation and (e) coal
430 consumption in *Energy* sector; (f) crop production in *Food* sector. Pink triangles in the

431 upper left sub-image represents the average of historical and simulation value in
432 1981-2020 of each province in the YRB.

433 We compared model performance during the historical period (1981–2020) against
434 historical data. These data are sourced from multiple channels, including statistical
435 yearbooks, hydrological stations, remote sensing observations, and outputs from other
436 models (Table S3).

437 For human sectors, the simulation accuracy of selected key variables from each
438 sector is consistently high ($R > 0.95$), including total population, gross domestic
439 product (GDP), water withdrawal, electricity generation, coal consumption, and crop
440 production across the nine provinces (Fig.11). However, the accuracy varies among
441 provinces, particularly for GDP, electricity generation, coal consumption, and crop
442 production. Some provinces, like Neimeng, exhibit lower simulation accuracy for
443 certain indicators than others, probably due to the simplification of relevant modelled
444 processes, imperfect parameterizations, and external policy interventions. Among all
445 sectors, the greatest uncertainty arises in simulating coal consumption, because the
446 absence of a clear historical trend results in poor fitting performance. Nevertheless, the
447 model performs reasonably well in the human sectors, effectively capturing the
448 historical dynamics of human systems in the YRB.



449

450 Fig.12 Validation of the natural system processes during historical period of 1981-
 451 2020. (a) runoff in *Water Supply* sector; (b) sediment load in *Sediment* sector; (c)
 452 forest area in *Land* sector, and the historical dataset is discontinuous; (d) net primary
 453 productivity in *Carbon* sector. Pink triangles in the upper left sub-image represents
 454 the average of historical and simulation value in 1981-2020 of each sub-basin in the
 455 YRB.

456 For natural sectors, the simulation accuracy for runoff, sediment load, forest area,
 457 and NPP in the YRB is relatively high ($R > 0.7$) (Fig.12). At the sub-basin level, the
 458 overall performance is satisfactory; however, the model shows lower accuracy in
 459 simulating sediment transport in the mid- and downstream. Compared to the human
 460 sectors, the natural sectors generally exhibit lower correlations with historical data,
 461 largely due to the simplifications required when modeling physically complex natural
 462 processes. Nevertheless, the model is still capable of capturing the historical dynamics
 463 of natural processes in the YRB.

464 Sensitivity analyses with randomly generated parameter values reveal growing

465 uncertainty in the long-term trajectories of socio-economic and natural variables; the
 466 model maintains behavioral robustness across all runs without catastrophic collapse or
 467 unrealistic oscillations (see Supporting Information S3 for details).

468 **3.2 Model application for future projection**

469 **3.2.1 Future baseline scenario**

470 The future baseline scenario represents a trajectory in which existing plans and
 471 policies continue to operate without substantial changes in external environments. The
 472 development of the baseline scenario primarily relies on variables from the *Population*,
 473 *Economy*, *Water Demand*, and *Land* sector based on available government planning
 474 documents, historical trends, and other projections (Table 2). For future projections,
 475 variables or parameters not specified in the table are held constant at historical levels
 476 from their most recent year. Future climate data (2015-2100) are from the ensemble
 477 mean of 11 CMIP6 models (ACCESS-CM2, CESM2, CMCC-ESM2, GFDL-ESM4,
 478 INM-CM4-8, INM-CM5-0, IPSL-CM6A-LR, MIROC6, MRI-ESM2-0, UKESM1-0-
 479 LL, and HadGEM-GC31-LL) (available at
 480 <https://cds.climate.copernicus.eu/datasets/projections-cmip6?tab=download>) for the
 481 SSP 2-4.5 because this scenario aligns more closely with the climate trends in the YRB.
 482 To ensure temporal consistency, CMIP6 historical climate data (1981–2014) were used
 483 instead of observed historical records. To reduce systemic biases in the raw CMIP6 data,
 484 we applied bias correction using CN05 and ground weather stations observations from
 485 1981 to 2014. By statistically aligning the mean of the CMIP6 data with observation
 486 records, systemic bias is removed while retaining the temporal consistency required for
 487 long-term simulation.

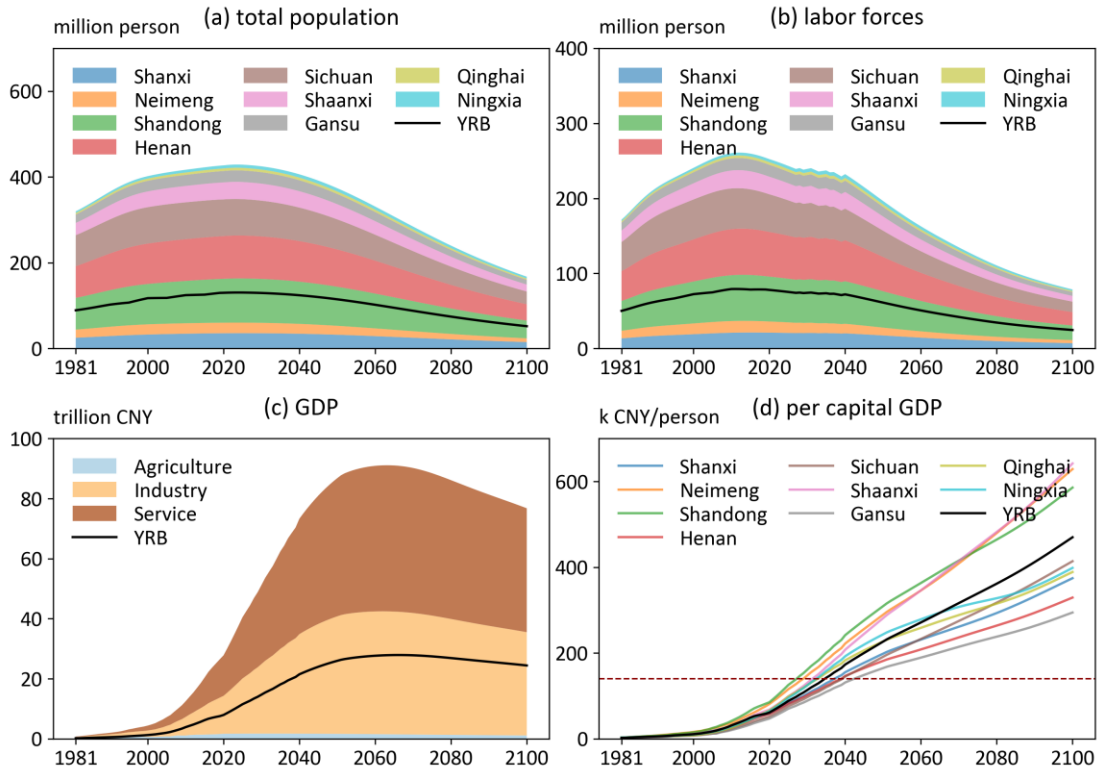
488 We run the model under the future baseline scenario to project the evolution of
 489 CHANS in the basin from 2021 to 2100 (see Supporting Information S6 for details of
 490 future scenario design and supplementary spreadsheet for exogenous variables).

491 Table 2 Settings of key variables in the future baseline scenario

Sector	Variables	Future baseline
--------	-----------	-----------------

Population	• Total fertility	• 2024 United Nations Population Projections
	• Gender ratio	• 2024 United Nations Population Projections
	• Average years of schooling	• The national maximum in 2023 (Germany) as the upper limit
	• Urban and rural population ratio	• Analysis and Forecast of Urbanization Trends in China's Modernization by 2020
	• Labor force	• Delay retirement age
Energy	• Electricity generation sources ratio	• Projected provincial-level energy structure meeting China's carbon peaking and carbon neutrality goals (Li et al., 2024)
	• Irrigation intensity	• Irrigation water use intensity declines linearly (1%/yr) to its minimum value.
Water Demand	• Industry, service, livestock water use intensity	• Industry, service and livestock water use intensity declines linearly (1%/yr) to its minimum value.
Land	• Land use area	• Cropland, forest, and grassland are allowed to be converted into each other, but not to unused land; unused land can be converted to the rest land; wetlands are fixed.
		• Minimum cropland area above the red line for cropland protection.
Climate	• Temperature	• SSP 2-4.5 — CMIP 6
	• Precipitation	
	• Potential evapotranspiration	
	• Precipitation intensity	
	• CO ₂ concentration,	

492 **3.2.2 Projection of CHANS dynamics in future baseline scenario**

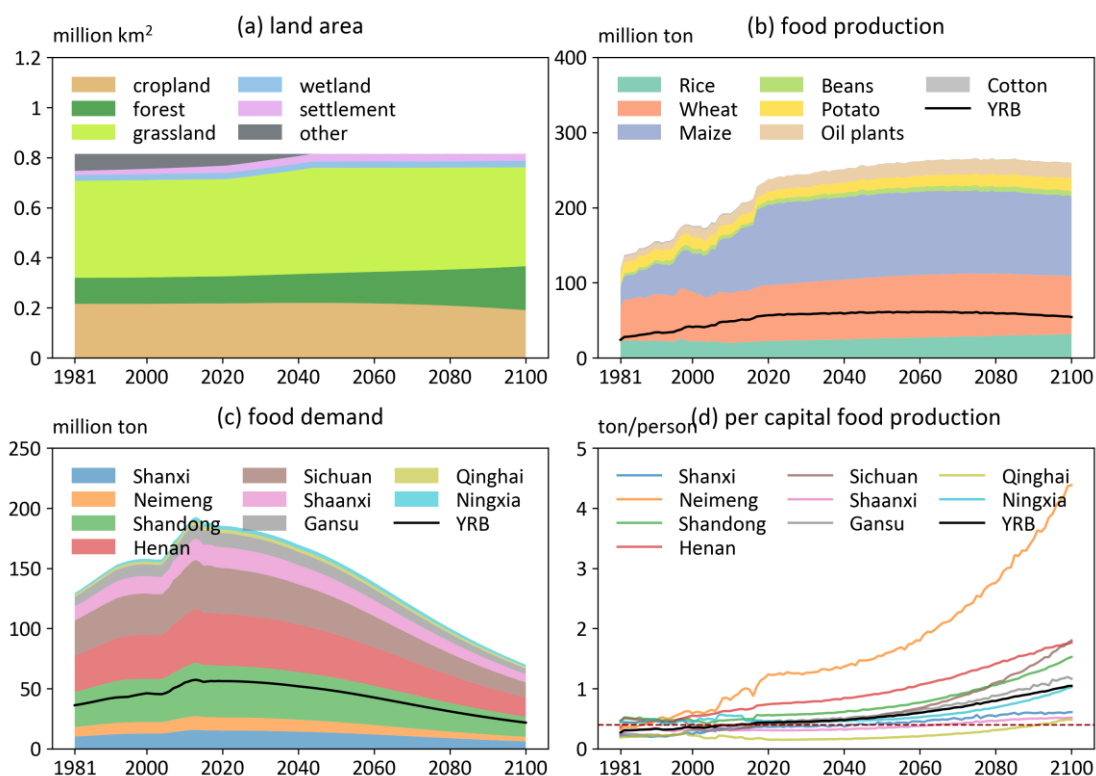


493

494 Fig.13 Changes in key variables of the *Population* and *Economy* sector in the future
 495 baseline scenario: (a) the total population, (b) the total labor forces, (c) the gross
 496 output of agriculture, industry, and service, and the total gross domestic output, (d) the
 497 per capita GDP in nine provinces and YRB.

498 The model simulates human and natural system dynamics under the future
 499 baseline scenario and produces outputs for nine provinces and their corresponding areas
 500 within the YRB. The simulation results are reported either at the provincial level (nine
 501 provinces) for human system sectors or at the basin level (basin boundary) for natural
 502 system sectors. The total population in the nine provinces and the YRB is projected to
 503 peak in 2023 and 2024, at 429 million and 131 million, respectively, driven by declining
 504 fertility rates (Fig.13 (a)). The labor force peaks earlier, reaching 261 million in the nine
 505 provinces in 2012 and 79 million in the YRB in 2011 (Fig.13 (b)). After 2025, the labor
 506 force is projected to increase again due to the delayed retirement policy. GDP in the
 507 nine provinces is expected to increase until a peak in 2063, at 91 trillion CNY (three

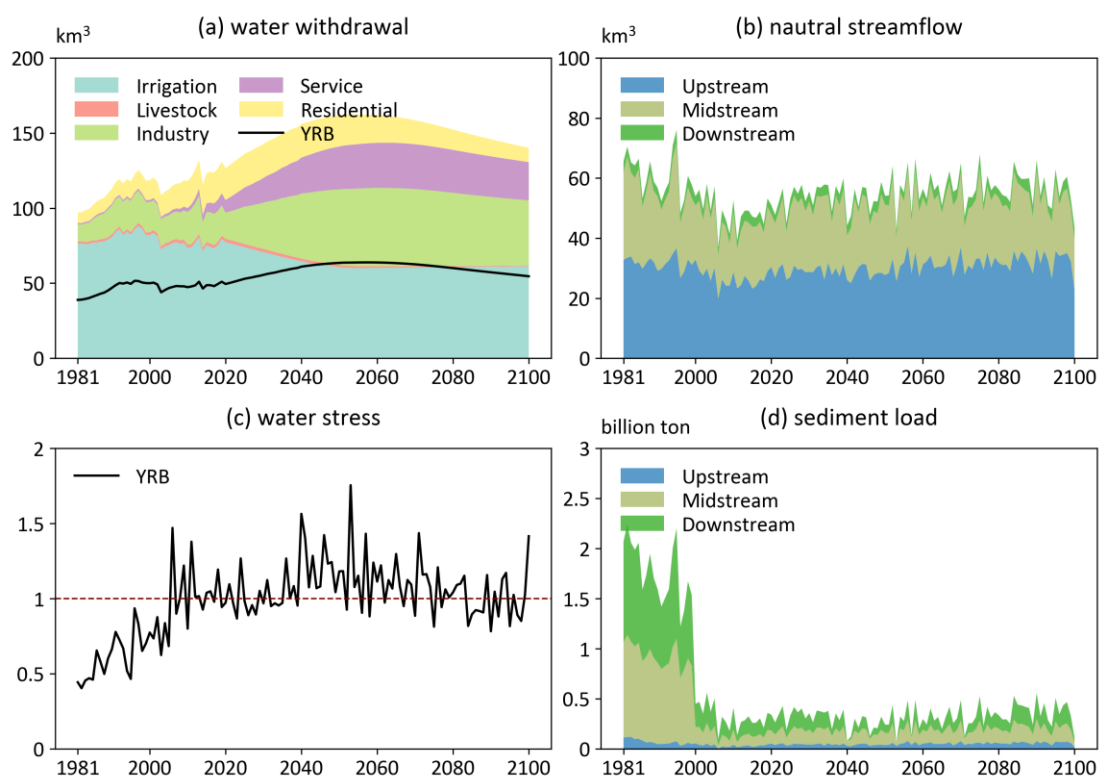
508 times the 2020 level, in 2020 constant prices), under the influence of a labor force
 509 decline, with the YRB reaching its peak four years later (Fig.13 (c)). In contrast to total
 510 GDP, per capita GDP in all regions is projected to continue rising throughout the future
 511 period (Fig.13 (d)). Although all provinces demonstrate improvements in economic
 512 status and living standards, considerable regional disparities persist. Among the nine
 513 provinces, Shaanxi demonstrates the largest growth in average per capita GDP from
 514 2021 to 2100 relative to the historical period (1981-2020), with a more than
 515 seventeenfold increase, while the YRB as a whole shows an over thirteenfold increase.



516
 517 Fig.14 Land and food in the future baseline scenario. (a) land area in the YRB; (b-d)
 518 food production of seven crop types, food demand and per capita food production in
 519 nine provinces and the YRB, red dotted line represents the 0.4 tons international food
 520 security threshold.

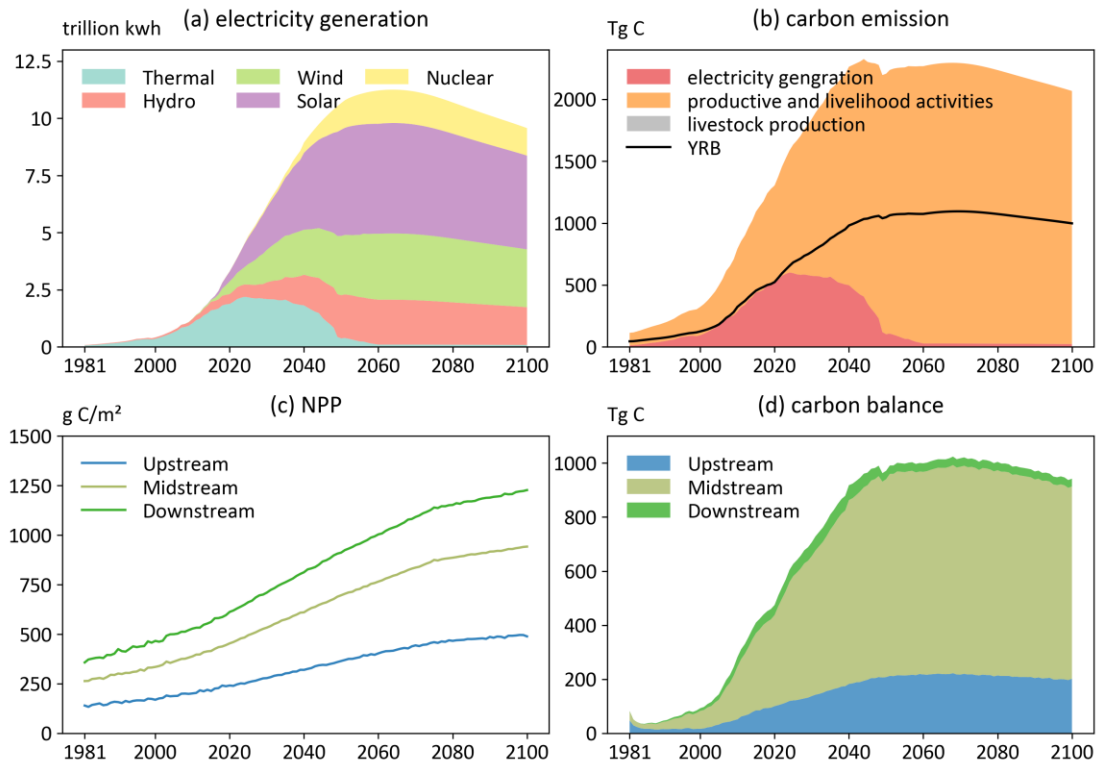
521 Under the future baseline scenario, land use patterns remain relatively stable based
 522 on historical trends (Fig. 14(a)), as no new land use policies are introduced and cropland
 523 area in each province has to stay above a mandatory minimum threshold for food

524 security (China's Cropland Red Line policy). The forest area is projected to increase
 525 gradually, reaching 62% above the 2021 level by 2100, while the cropland area is
 526 expected continue declining, falling 12% below the 2021 level. Total crop production
 527 in nine provinces and YRB is projected to peak in 2079 and 2062 (Fig.14 (b)),
 528 respectively, driven by the combined effects of declining cropland area and increasing
 529 crop yields. Food demand in both the nine provinces and the YRB as a whole peaked
 530 in 2013 (193 million tons and 57 million tons, respectively) (Fig.14 (c)), largely driven
 531 by population dynamics. In the future, per capita food production in the YRB is
 532 projected to consistently exceed the international food security threshold of 0.4 tons per
 533 person (Fig.14 (d)). However, in certain years, provinces such as Qinghai and Shaanxi
 534 could fall below this standard.



535
 536 Fig.15 Water demand and supply in the future baseline scenario. (a) water withdrawal
 537 across five water-use sectors in nine provinces and the YRB; (b) natural streamflow in
 538 up-, mid- and downstream; (c) water stress in the YRB, red dotted line represents the
 539 water security threshold; (d) sediment load in the up-, mid- and downstream.

540 Total water withdrawal in the nine provinces and the YRB is projected to peak in
541 2056 and 2058, reaching 162 km³ and 64 km³, respectively (Fig.15 (a)). Irrigation water
542 withdrawal is expected to decline, driven by reductions in cropland area and irrigation
543 intensity, the latter resulting from improvements in irrigation efficiency assumed in the
544 scenario. Peaks in residential, industrial, service, and livestock water withdrawals are
545 primarily associated with projected peaks in population and GDP. Natural streamflow
546 is projected to exhibit a fluctuating upward trend of 0.073 km³/year basin-wide (Fig.
547 15(b)), with the most significant growth in the upstream region (0.068 km³/year).
548 Considering the ecological flow requirement of 18.7 km³ (YRCCMWR, 2015), water
549 stress (calculated as water consumption divided by (natural discharge - ecological flow))
550 is expected to decline in the latter half of the century, largely due to the peak and
551 subsequent reduction in water withdrawal. However, overall water stress is projected
552 to exceed historical levels in 2041 and will fall below 1 in 38% of the years (Fig.15 (c)),
553 reflecting persistent human–water tensions and future trade-offs between ecological
554 and human water use. As a result of reduced actual streamflow, sediment transport in
555 the Yellow River is projected to decline sharply (Fig.15 (d)), with a 71% decrease in
556 sediment load relative to the historical period.



557

558

559

560

561

562

563

564

565

566

567

568

569

570

571

572

573

Fig.16 Electricity and carbon in the future baseline scenario. (a) the electricity generation from five sources in nine provinces; (b) carbon emission from three sources in nine provinces and the YRB; (c-d) the net primary productivity and carbon balance in the up-, mid-, and downstream.

Since the energy system is transitioning to carbon neutrality goals under the future baseline scenario, thermal power generation is projected to decline sharply, while clean energy (hydropower, wind, solar, and nuclear) will become the dominant source for electricity generation (Fig.16 (a)). The large-scale adoption of clean energy will lead to a peak in carbon emissions from electricity generation in 2024 (Fig.16 (b)). In contrast, emissions from productive and livelihood activities are projected to rise substantially over time, with total human emissions in the YRB reaching a peak in 2044. NPP is anticipated to increase markedly in response to CO₂ concentration increase (Fig.16 (c)). Although the carbon balance of the YRB has remained positive (net carbon source), it is expected to gradually decline after 2068 (Fig.16 (d)), indicating that the basin's ecosystems alone cannot fully offset human-induced carbon emissions.

The above projections of future baseline scenarios highlight persistent challenges

574 to achieving sustainable development in the YRB, underscoring the need for integrated
575 policy responses to address these challenges. Priority should be given to enhancing
576 water-use efficiency and establishing adaptive water resource allocation mechanisms
577 that balance ecological and human water needs. Sediment management strategies,
578 which combine ecological restoration with hydraulic regulation, are necessary to
579 maintain river stability and delta health. To counter the decline in labor force, policies
580 should promote industrial upgrading and technological innovation. Strengthening the
581 basin's carbon mitigation capacity requires accelerating the clean energy transition and
582 expanding ecological restoration to enhance carbon sequestration. Finally, a multi-
583 sectoral, CHANS-based governance framework should be established to coordinate
584 water, land, energy, and carbon management, enabling evidence-based scenario
585 analysis and adaptive policy design for long-term sustainability.

586 **4 Discussion and conclusions**

587 The development of the CHANS-SD-YRB model involves a series of key
588 considerations in translating a conceptual framework into a functioning model. The
589 framework focuses on human–water interactions in the YRB, integrating bidirectional
590 feedback between human and natural processes. SD was chosen to implement the
591 framework, as it effectively captures feedback, non-linear relationships, and cross-
592 sectoral linkages within complex human–natural systems, while remaining practical
593 and straightforward to use. For quantitative representation of human–natural processes,
594 we prefer theoretical methods that incorporate key interactions within the system
595 suitable for implementation using SD. For example, the Budyko framework connects
596 the *Land*, *Climate*, *Water Demand*, and *Water Supply* sectors. Relative to distributed
597 hydrological models, it offers lower computational complexity and reduced data
598 requirements. The Cobb–Douglas production function links the *Population* and
599 *Economy* sectors. Compared with Computable General Equilibrium models (Fujimori
600 et al., 2014a), it is simpler to construct and requires fewer parameters and data inputs.
601 When no suitable theoretical framework/method is available to describe a process, we

602 rely on empirical relationships derived from historical data. For example, crop yields
603 are estimated using fitted relationships between climate variables, fertilizer application,
604 and historical yields. For processes that cannot be represented through empirical
605 functions, we apply literature-based estimates to obtain approximate quantitative
606 relationships, such as fossil fuel emission factors. For processes influenced by external
607 drivers that cannot be endogenously expressed within the model, we quantify them
608 using exogenous parameters derived from historical statistics, such as water intensity.
609 Given the heterogeneous human–natural interactions in the YRB, we represent all
610 processes at the provincial and sub-basin scales using scale-specific parameters, except
611 where parameters or data at these levels are unavailable.

612 The CHANS-SD-YRB model explicitly couples multiple human and natural
613 sectors, enabling a more integrated representation of feedbacks across population,
614 economy, energy, food, water, sediment, land, carbon, and climate. Unlike models that
615 focus on specific sectors or isolated subsystems—such as eco-hydrological models and
616 sediment transport models, which may well capture individual processes but cannot
617 represent the complex human–nature interactions driving system dynamics. Our
618 model’s integration of human and natural sectors provides a robust framework for
619 addressing regional CHANS challenges and offers practical guidance for sustainable
620 development. The CHANS-SD-YRB model serves as a comprehensive platform for
621 conducting system dynamics prediction, scenario analysis, policy evaluation, and
622 optimization, to alleviate human–water conflicts, ensure food security, and achieve
623 long-term sustainability. For example, analysis of the impacts of the 1987 Yellow River
624 water allocation policy (Song et al., 2024) offer valuable insights for adjusting
625 interprovincial water distribution to promote sustainable water governance; assessment
626 of ecological restoration policies (Li et al., 2015) can guide future ecological
627 engineering; spatiotemporal dynamics of future water gaps can serve as a valuable
628 reference for planning inter-basin water transfers. The model’s flexibility also allows
629 for the incorporation of additional feedback, for example, linking water scarcity to

630 industrial output or climate warming to agricultural productivity. These could include
631 the effects of global warming on human health (Yin et al., 2023a) and economic
632 activities (Nordhaus, 2017), water constraints on production, dietary shifts influencing
633 carbon emissions and land use (Ren et al., 2023), and the trade-offs between carbon
634 mitigation and food security (Xu et al., 2022).

635 Nevertheless, the model remains subject to further refinement. The current
636 simplifications of natural processes could be replaced with more sophisticated models
637 to enhance simulation accuracy. For instance, the YRB hydrological processes involve
638 highly complex human interventions, including reservoir, conservation, and
639 revegetation projects (Wang et al., 2025). The refined runoff simulations by distributed
640 hydrological models improve water supply assessments through their better
641 characterization of spatial heterogeneity in soil, precipitation, and snowmelt (Cong et
642 al., 2009). For human processes, the *Energy* and *Economy* sectors could be refined to
643 model more detailed industry subsectors and emerging trends in energy demand driven
644 by electrification. Given the uncertainty in future climate change, the sensitivity of the
645 system's future projections to alternative climate change scenarios (SSP1-2.6, SSP3-
646 7.0, or SSP5-8.5) warrants exploration. Moreover, there are still important feedbacks
647 absent from the current coupling framework. Notable examples include the effects of
648 land use change on climate, the effects of climate change on economic growth, and the
649 effects of pricing on energy use and carbon emissions. These missing feedbacks could
650 be incorporated based on recent studies, including the land use feedback on
651 precipitation through moisture recycling (Sang et al., 2025a), socioeconomic losses
652 from impacts of climate change and extremes (Waidelich et al., 2024b), and integration
653 with Computable General Equilibrium (CGE) models (Fujimori et al., 2014b). In
654 particular, recent modeling work by Wells et al. (2026) demonstrated that a more
655 comprehensive representation of climate-to-society feedbacks is possible within the
656 system dynamics framework. Additionally, the model's spatial and temporal resolutions
657 are relatively coarse due to the inherent mismatch in spatiotemporal scales between

658 human and natural processes. The scale at which we make the model represents a
659 practical compromise, constrained by data availability and aligned with the study's
660 objectives. Simulations at finer scales (e.g., monthly, daily, or gridded) would enhance
661 the representation of natural processes (e.g., hydrological processes, land use changes,
662 and food production) and the associated spatiotemporal heterogeneity (e.g., daily
663 simulations can assess the impacts of extreme weather). However, it may also
664 exacerbate the scale mismatch with socioeconomic processes, making it challenging to
665 analyze cross-sectoral dynamics. Technically, the inherent limitations of the SD
666 software restrict the model's ability to represent temporal fluctuations and spatial
667 variations. To overcome this, transitioning from the VENSIM platform to a code-based
668 implementation will be necessary, which would also facilitate coupling with other
669 models. Future research should prioritize these improvements to strengthen both the
670 performance and applicability of the model.

671 Drawing on the conceptual framework of Sang et al. (2025), this study implements
672 it into a fully functional, validated System Dynamics model tool, CHANS-SD-YRB 1.0.
673 The model fills the gap in CHANS modeling for the YRB. It integrates the dynamics
674 of ten interconnected sectors: *Population, Economy, Energy, Food, Water Demand,*
675 *Water Supply, Sand, Land, Carbon, and Climate*, achieving reciprocal feedback
676 between human and natural systems. This model can serve as a robust tool to inform
677 policy decisions that influence the evolution of coupled human–natural systems and to
678 explore pathways for optimizing these systems toward sustainability. Furthermore, the
679 modeling process provides valuable experience for regional CHANS modeling and
680 contributes to advancing the broader development of CHANS models at the regional
681 scale.

682 **Code and data availability**

683 The CHANS-SD-YRB V1.0 model (Vensim DSS format), along with the input
684 data and simulation outputs used in this study, are openly accessible at
685 <https://doi.org/10.5281/zenodo.17568962> (Sang, 2025), and

686 https://github.com/sangshan-ss/CHANS_SD_YRB.

687 **Author contributions**

688 Conceptualization: YL, SS¹, BF. Data curation: SS¹. Formal analysis: SS¹.
689 Funding acquisition: BF, YL. Investigation: YL, SS¹. Methodology: SS¹, YL, BF.
690 Project administration: YL. Resources: YL. Software: SS¹, SZ, LY. Supervision: YL,
691 BF. Validation: SS¹, SZ, LY. Visualization: SS¹. Writing – original draft: SS¹. Writing –
692 review and editing: SS¹, YL, SW, YXL, XTW, SS², WZ, XHW. (Note: SS¹ refers to
693 Shan Sang, and SS² refers to Shuang Song, to distinguish between authors with identical
694 initials.)

695 **Competing interests**

696 The authors declare that they have no conflict of interest.

697 **Acknowledgements**

698 We thank Dr. Weishuang Qu for developing the Threshold 21 model in the
699 Millennium Institute that inspired this study, and also for his and Dr. Haiyan Jiang's
700 generous help with the CHANS-SD-YRB modeling. We also thank the data support
701 from Dr. Xianghui Kong, and National Earth System Science Data Center, National
702 Science & Technology Infrastructure of China (<http://www.geodata.cn>).

703 **Financial support**

704 This study is supported by the National Natural Science Foundation of China
705 (Grant No. 42041007), and the Fundamental Research Funds for the Central
706 Universities.

707 **References:**

708 Allen, C., Metternicht, G., Wiedmann, T., and Pedercini, M.: Greater gains for Australia
709 by tackling all SDGs but the last steps will be the most challenging, *Nat Sustain*, 2,
710 1041–1050, <https://doi.org/10.1038/s41893-019-0409-9>, 2019.

711 Breach, P. A. and Simonovic, S. P.: ANEMI3: An updated tool for global change
712 analysis, *PLoS ONE*, 16, e0251489, <https://doi.org/10.1371/journal.pone.0251489>,
713 2021.

714 Calvin, K. and Bond-Lamberty, B.: Integrated human-earth system modeling—state of

715 the science and future directions, *Environ. Res. Lett.*, 13, 063006,
716 <https://doi.org/10.1088/1748-9326/aac642>, 2018.

717 Changming, L. and Shifeng, Z.: Drying up of the yellow river: its impacts and counter-
718 measures, *Mitigation and Adaptation Strategies for Global Change*, 7, 203–214,
719 <https://doi.org/10.1023/A:1024408310869>, 2002.

720 Cheng, Y., Huang, M., Lawrence, D. M., Calvin, K., Lombardozzi, D. L., Sinha, E.,
721 Pan, M., and He, X.: Future bioenergy expansion could alter carbon sequestration
722 potential and exacerbate water stress in the United States, *Science Advances*, 8,
723 eabm8237, <https://doi.org/10.1126/sciadv.abm8237>, 2022.

724 Cobb, C. W. and Douglas, P. H.: A theory of production, *The American Economic*
725 *Review*, 18, 139–165, 1928.

726 Cong, Z., Yang, D., Gao, B., Yang, H., and Hu, H.: Hydrological trend analysis in the
727 Yellow River basin using a distributed hydrological model, *Water Resources Research*,
728 45, 2008WR006852, <https://doi.org/10.1029/2008WR006852>, 2009.

729 Cui, T., Wang, Y., Sun, R., Qiao, C., Fan, W., Jiang, G., Hao, L., and Zhang, L.:
730 Estimating Vegetation Primary Production in the Heihe River Basin of China with
731 Multi-Source and Multi-Scale Data, *PLOS ONE*, 11, e0153971,
732 <https://doi.org/10.1371/journal.pone.0153971>, 2016.

733 Davies, E. G. R. and Simonovic, S. P.: ANEMI: a new model for integrated assessment
734 of global change, *Interdisciplinary Environmental Review*, 2011.

735 Di Vittorio, A. V., Sinha, E., Hao, D., Singh, B., Calvin, K. V., Shippert, T., Patel, P.,
736 and Bond-Lamberty, B.: E3SM-GCAM: A Synchronously Coupled Human Component
737 in the E3SM Earth System Model Enables Novel Human-Earth Feedback Research,
738 *Journal of Advances in Modeling Earth Systems*, 17, e2024MS004806,
739 <https://doi.org/10.1029/2024MS004806>, 2025.

740 Dobbs, G. R., Liu, N., Caldwell, P. V., Miniati, C. F., Sun, G., Duan, K., and Bolstad, P.
741 V.: Inter-basin surface water transfers database for public water supplies in
742 conterminous United States, 1986–2015, *Sci Data*, 10, 255,
743 <https://doi.org/10.1038/s41597-023-02148-5>, 2023.

744 Dottori, F., Szewczyk, W., Ciscar, J.-C., Zhao, F., Alfieri, L., Hirabayashi, Y., Bianchi,
745 A., Mongelli, I., Frieler, K., Betts, R. A., and Feyen, L.: Increased human and economic
746 losses from river flooding with anthropogenic warming, *Nature Clim Change*, 8, 781–
747 786, <https://doi.org/10.1038/s41558-018-0257-z>, 2018.

748 EEA: Trends in atmospheric concentrations of CO₂ (ppm), CH₄ (ppb) and N₂O (ppb),
749 between 1800 and 2017, 2019.

- 750 Feng, X., Fu, B., Piao, S., Wang, S., Ciais, P., Zeng, Z., Lü, Y., Zeng, Y., Li, Y., Jiang,
751 X., and Wu, B.: Revegetation in China's Loess Plateau is approaching sustainable water
752 resource limits, *Nature Clim Change*, 6, 1019–1022,
753 <https://doi.org/10.1038/nclimate3092>, 2016.
- 754 Feng, Y. and Zhu, A.: Spatiotemporal differentiation and driving patterns of water
755 utilization intensity in Yellow River Basin of China: Comprehensive perspective on the
756 water quantity and quality, *Journal of Cleaner Production*, 369, 133395,
757 <https://doi.org/10.1016/j.jclepro.2022.133395>, 2022.
- 758 Flörke, M., Kynast, E., Bärlund, I., Eisner, S., Wimmer, F., and Alcamo, J.: Domestic
759 and industrial water uses of the past 60 years as a mirror of socio-economic
760 development: A global simulation study, *Global Environmental Change*, 23, 144–156,
761 <https://doi.org/10.1016/j.gloenvcha.2012.10.018>, 2013.
- 762 Forrester, J. W.: *Principles of systems*, Pegasus Communications, Inc, Waltham, MA,
763 1968.
- 764 Fu, B. and Li, Y.: Bidirectional coupling between the Earth and human systems is
765 essential for modeling sustainability, *National Science Review*, 3, 397–398,
766 <https://doi.org/10.1093/nsr/nww094>, 2016.
- 767 Fu, B., Liu, Y., Lü, Y., He, C., Zeng, Y., and Wu, B.: Assessing the soil erosion control
768 service of ecosystems change in the Loess Plateau of China, *Ecological Complexity*, 8,
769 284–293, <https://doi.org/10.1016/j.ecocom.2011.07.003>, 2011.
- 770 Fu, B., Liu, Y., and Meadows, M. E.: Ecological restoration for sustainable
771 development in China, *National Science Review*, 10, nwad033,
772 <https://doi.org/10.1093/nsr/nwad033>, 2023.
- 773 Fujimori, S., Masui, T., and Matsuoka, Y.: Development of a global computable general
774 equilibrium model coupled with detailed energy end-use technology, *Applied Energy*,
775 128, 296–306, <https://doi.org/10.1016/j.apenergy.2014.04.074>, 2014a.
- 776 Fujimori, S., Masui, T., and Matsuoka, Y.: Development of a global computable general
777 equilibrium model coupled with detailed energy end-use technology, *Applied Energy*,
778 128, 296–306, <https://doi.org/10.1016/j.apenergy.2014.04.074>, 2014b.
- 779 Fujimori, S., Wu, W., Doelman, J., Frank, S., Hristov, J., Kyle, P., Sands, R., van Zeist,
780 W.-J., Havlik, P., Domínguez, I. P., Sahoo, A., Stehfest, E., Tabeau, A., Valin, H., van
781 Meijl, H., Hasegawa, T., and Takahashi, K.: Land-based climate change mitigation
782 measures can affect agricultural markets and food security, *Nat Food*, 3, 110–121,
783 <https://doi.org/10.1038/s43016-022-00464-4>, 2022.
- 784 Gou, J., Miao, C., Samaniego, L., Xiao, M., Wu, J., and Guo, X.: CNRD v1.0: A High-

785 Quality Natural Runoff Dataset for Hydrological and Climate Studies in China, *Bulletin*
786 of the American Meteorological Society, 102, E929–E947,
787 <https://doi.org/10.1175/BAMS-D-20-0094.1>, 2021.

788 Hasegawa, T., Sakurai, G., Fujimori, S., Takahashi, K., Hijioka, Y., and Masui, T.:
789 Extreme climate events increase risk of global food insecurity and adaptation needs,
790 *Nat Food*, 2, 587–595, <https://doi.org/10.1038/s43016-021-00335-4>, 2021.

791 Hyun, J.-Y., Huang, S.-Y., Yang, Y.-C. E., Tidwell, V., and Macknick, J.: Using a
792 coupled agent-based modeling approach to analyze the role of risk perception in water
793 management decisions, *Hydrology and Earth System Sciences*, 23, 2261–2278,
794 <https://doi.org/10.5194/hess-23-2261-2019>, 2019.

795 Jain, S., Mindlin, J., Koren, G., Gulizia, C., Steadman, C., Langendijk, G. S., Osman,
796 M., Abid, M. A., Rao, Y., and Rabanal, V.: Are We at Risk of Losing the Current
797 Generation of Climate Researchers to Data Science?, *AGU Advances*, 3,
798 e2022AV000676, <https://doi.org/10.1029/2022AV000676>, 2022.

799 Jia, K., Liang, S., Liu, S., Li, Y., Xiao, Z., Yao, Y., Jiang, B., Zhao, X., Wang, X., Xu,
800 S., and Cui, J.: Global Land Surface Fractional Vegetation Cover Estimation Using
801 General Regression Neural Networks From MODIS Surface Reflectance, *IEEE*
802 *Transactions on Geoscience and Remote Sensing*, 53, 4787–4796,
803 <https://doi.org/10.1109/TGRS.2015.2409563>, 2015.

804 Jia, K., Yang, L., Liang, S., Xiao, Z., Zhao, X., Yao, Y., Zhang, X., Jiang, B., and Liu,
805 D.: Long-Term Global Land Surface Satellite (GLASS) Fractional Vegetation Cover
806 Product Derived From MODIS and AVHRR Data, *IEEE Journal of Selected Topics in*
807 *Applied Earth Observations and Remote Sensing*, 12, 508–518,
808 <https://doi.org/10.1109/JSTARS.2018.2854293>, 2019.

809 Jiang, H., Simonovic, S. P., and Yu, Z.: ANEMI_Yangtze v1.0: a coupled human–
810 natural systems model for the Yangtze Economic Belt – model description, *Geosci.*
811 *Model Dev.*, 26, 2022.

812 Kemei, Z., Rotich, T., and Bitok, J.: Modelling population dynamics using age-
813 structured system of partial differential equations, *IJAMR*, 13, 110–116,
814 <https://doi.org/10.14419/m81azj37>, 2024.

815 Li, M., Shan, R., Abdulla, A., Virguez, E., and Gao, S.: The role of dispatchability in
816 China’s power system decarbonization, *Energy Environ. Sci.*, 17, 2193–2205,
817 <https://doi.org/10.1039/D3EE04293F>, 2024.

818 Li, X., Cheng, G., Lin, H., Cai, X., Fang, M., Ge, Y., Hu, X., Chen, M., and Li, W.:
819 Watershed System Model: The Essentials to Model Complex Human-Nature System at

- 820 the River Basin Scale, *Journal of Geophysical Research: Atmospheres*, 123, 3019–3034,
821 <https://doi.org/10.1002/2017JD028154>, 2018.
- 822 Li, X., Zhang, L., Zheng, Y., Yang, D., Wu, F., Tian, Y., Han, F., Gao, B., Li, H., Zhang,
823 Y., Ge, Y., Cheng, G., Fu, B., Xia, J., Song, C., and Zheng, C.: Novel hybrid coupling
824 of ecohydrology and socioeconomy at river basin scale: A watershed system model for
825 the Heihe River basin, *Environmental Modelling & Software*, 141, 105058,
826 <https://doi.org/10.1016/j.envsoft.2021.105058>, 2021.
- 827 Li, Z., Liu, X., Niu, T., Kejia, D., Zhou, Q., Ma, T., and Gao, Y.: Ecological Restoration
828 and Its Effects on a Regional Climate: The Source Region of the Yellow River, China,
829 *Environ. Sci. Technol.*, 49, 5897–5904, <https://doi.org/10.1021/es505985q>, 2015.
- 830 Liu, C., Golding, D., and Gong, G.: Farmers’ coping response to the low flows in the
831 lower Yellow River: A case study of temporal dimensions of vulnerability, *Global*
832 *Environmental Change*, 18, 543–553, <https://doi.org/10.1016/j.gloenvcha.2008.09.002>,
833 2008.
- 834 Liu, J.: Integration across a metacoupled world, *E&S*, 22, art29,
835 <https://doi.org/10.5751/ES-09830-220429>, 2017.
- 836 Liu, J., Dietz, T., Carpenter, S. R., Alberti, M., Folke, C., Moran, E., Pell, A. N.,
837 Deadman, P., Kratz, T., Lubchenco, J., Ostrom, E., Ouyang, Z., Provencher, W.,
838 Redman, C. L., Schneider, S. H., and Taylor, W. W.: Complexity of Coupled Human
839 and Natural Systems, *Science*, 317, 1513–1516,
840 <https://doi.org/10.1126/science.1144004>, 2007.
- 841 MAARA: China Agriculture Yearbook,
842 <https://data.cnki.net/yearBook?type=type&code=A>, 2020.
- 843 Miao, C., Kong, D., Wu, J., and Duan, Q.: Functional degradation of the water–
844 sediment regulation scheme in the lower Yellow River: Spatial and temporal analyses,
845 *Science of The Total Environment*, 551–552, 16–22,
846 <https://doi.org/10.1016/j.scitotenv.2016.02.006>, 2016.
- 847 Miao, C., Gou, J., Fu, B., Tang, Q., Duan, Q., Chen, Z., Lei, H., Chen, J., Guo, J.,
848 Borthwick, A. G. L., Ding, W., Duan, X., Li, Y., Kong, D., Guo, X., and Wu, J.: High-
849 quality reconstruction of China’s natural streamflow, *Science Bulletin*, 67, 547–556,
850 <https://doi.org/10.1016/j.scib.2021.09.022>, 2022.
- 851 Monier, E., Paltsev, S., Sokolov, A., Chen, Y.-H. H., Gao, X., Ejaz, Q., Couzo, E.,
852 Schlosser, C. A., Dutkiewicz, S., Fant, C., Scott, J., Kicklighter, D., Morris, J., Jacoby,
853 H., Prinn, R., and Haigh, M.: Toward a consistent modeling framework to assess multi-
854 sectoral climate impacts, *Nat Commun*, 9, 1–8, <https://doi.org/10.1038/s41467-018->

855 02984-9, 2018.

856 Motesharrei, S., Rivas, J., Kalnay, E., Asrar, G. R., Busalacchi, A. J., Cahalan, R. F.,
857 Cane, M. A., Colwell, R. R., Feng, K., Franklin, R. S., Hubacek, K., Miralles-Wilhelm,
858 F., Miyoshi, T., Ruth, M., Sagdeev, R., Shirmohammadi, A., Shukla, J., Srebric, J.,
859 Yakovenko, V. M., and Zeng, N.: Modeling sustainability: population, inequality,
860 consumption, and bidirectional coupling of the Earth and Human Systems, *National*
861 *Science Review*, 3, 470–494, <https://doi.org/10.1093/nsr/nww081>, 2016.

862 NBSC: China Energy Statistical Yearbook,
863 <https://data.cnki.net/yearBook?type=type&code=A>, 2020a.

864 NBSC: China Population Census Yearbook,
865 <https://data.cnki.net/yearBook?type=type&code=A>, 2020b.

866 NBSC: China Statistical Yearbooks, <https://www.stats.gov.cn/english/>, 2020c.

867 Ning, X., Zhu, N., Liu, Y., and Wang, H.: Quantifying impacts of climate and human
868 activities on the grassland in the Three-River Headwater Region after two phases of
869 Ecological Project, *Geography and Sustainability*, 3, 164–176,
870 <https://doi.org/10.1016/j.geosus.2022.05.003>, 2022.

871 Nordhaus, W. D.: Revisiting the social cost of carbon, *Proceedings of the National*
872 *Academy of Sciences*, 114, 1518–1523, <https://doi.org/10.1073/pnas.1609244114>,
873 2017.

874 Qu, W., Shi, W., Zhang, J., and Liu, T.: T21 China 2050: A Tool for National Sustainable
875 Development Planning, *Geography and Sustainability*, 1, 33–46,
876 <https://doi.org/10.1016/j.geosus.2020.03.004>, 2020.

877 Rajah, J. K., Blanz, B., Kopainsky, B., and Schoenberg, W.: An endogenous modelling
878 framework of dietary behavioural change in the fully coupled human-climate FRIDA
879 v2.1 model, *Geoscientific Model Development*, 18, 5997–6022,
880 <https://doi.org/10.5194/gmd-18-5997-2025>, 2025.

881 Ren, M., Huang, C., Wu, Y., Deppermann, A., Frank, S., Havlík, P., Zhu, Y., Fang, C.,
882 Ma, X., Liu, Y., Zhao, H., Chang, J., Ma, L., Bai, Z., Xu, S., and Dai, H.: Enhanced
883 food system efficiency is the key to China’s 2060 carbon neutrality target, *Nat Food*, 4,
884 552–564, <https://doi.org/10.1038/s43016-023-00790-1>, 2023.

885 Richardson, G. P.: Reflections on the foundations of system dynamics, *System*
886 *Dynamics Review*, 27, 219–243, <https://doi.org/10.1002/sdr.462>, 2011.

887 Ristaino, J. B., Anderson, P. K., Bebbler, D. P., Brauman, K. A., Cunniffe, N. J., Fedoroff,
888 N. V., Finegold, C., Garrett, K. A., Gilligan, C. A., Jones, C. M., Martin, M. D.,

- 889 MacDonald, G. K., Neenan, P., Records, A., Schmale, D. G., Tateosian, L., and Wei, Q.:
890 The persistent threat of emerging plant disease pandemics to global food security,
891 *Proceedings of the National Academy of Sciences*, 118, e2022239118,
892 <https://doi.org/10.1073/pnas.2022239118>, 2021.
- 893 Rydzak, F., Obersteiner, M., Kraxner, F., Fritz, S., and McCallum, I.: FeliX3–Impact
894 Assessment Model: Systemic View across Societal Benefit Areas beyond Global Earth
895 Observation, Laxenburg: International Institute for Applied Systems Analysis (IIASA),
896 2013.
- 897 Sang, S.: CHANS-SD-YRB V1.0: A System Dynamics model of the coupled human-
898 natural systems for the Yellow River Basin (1.0.0),
899 <https://doi.org/10.5281/zenodo.17568963>, 2025.
- 900 Sang, S., Li, Y., Hou, C., Zi, S., and Lin, H.: The interprovincial green water flow in
901 China and its teleconnected effects on the social economy, *Hydrol. Earth Syst. Sci.*, 29,
902 67–84, <https://doi.org/10.5194/hess-29-67-2025>, 2025a.
- 903 Sang, S., Li, Y., Zong, S., Yu, L., Wang, S., Liu, Y., Wu, X., Song, S., Wang, X., and Fu,
904 B.: The modeling framework of the coupled human and natural systems in the Yellow
905 River Basin, *Geography and Sustainability*, 6, 100294,
906 <https://doi.org/10.1016/j.geosus.2025.100294>, 2025b.
- 907 Shan, Y., Guan, D., Zheng, H., Ou, J., Li, Y., Meng, J., Mi, Z., Liu, Z., and Zhang, Q.:
908 China CO₂ emission accounts 1997–2015, *Sci Data*, 5, 170201,
909 <https://doi.org/10.1038/sdata.2017.201>, 2018.
- 910 Song, S., Wen, H., Wang, S., Wu, X., Cumming, G. S., and Fu, B.: Quantifying the
911 effects of institutional shifts on water governance in the Yellow River Basin: A social-
912 ecological system perspective, *Journal of Hydrology*, 629, 130638,
913 <https://doi.org/10.1016/j.jhydrol.2024.130638>, 2024.
- 914 Vaidyanathan, G.: Integrated assessment climate policy models have proven useful,
915 with caveats, *Proc. Natl. Acad. Sci. U.S.A.*, 118, e2101899118,
916 <https://doi.org/10.1073/pnas.2101899118>, 2021.
- 917 Ventana Systems, Inc.: Vensim DSS (version 9.3), 2023.
- 918 Verburg, P. H., Dearing, J. A., Dyke, J. G., Leeuw, S. van der, Seitzinger, S., Steffen,
919 W., and Syvitski, J.: Methods and approaches to modelling the Anthropocene, *Global
920 Environmental Change*, 39, 328–340, <https://doi.org/10.1016/j.gloenvcha.2015.08.007>,
921 2016.
- 922 van Vliet, J.: Direct and indirect loss of natural area from urban expansion, *Nat Sustain*,
923 2, 755–763, <https://doi.org/10.1038/s41893-019-0340-0>, 2019.

- 924 Waidelich, P., Batibeniz, F., Rising, J., Kikstra, J. S., and Seneviratne, S. I.: Climate
 925 damage projections beyond annual temperature, *Nat. Clim. Chang.*, 14, 592–599,
 926 <https://doi.org/10.1038/s41558-024-01990-8>, 2024a.
- 927 Waidelich, P., Batibeniz, F., Rising, J., Kikstra, J. S., and Seneviratne, S. I.: Climate
 928 damage projections beyond annual temperature, *Nat. Clim. Chang.*, 14, 592–599,
 929 <https://doi.org/10.1038/s41558-024-01990-8>, 2024b.
- 930 Wang, M., Sun, R., Zhu, A., and Xiao, Z.: Evaluation and Comparison of Light Use
 931 Efficiency and Gross Primary Productivity Using Three Different Approaches, *Remote
 932 Sensing*, 12, 1003, <https://doi.org/10.3390/rs12061003>, 2020a.
- 933 Wang, S., Fu, B., Piao, S., Lü, Y., Ciais, P., Feng, X., and Wang, Y.: Reduced sediment
 934 transport in the Yellow River due to anthropogenic changes, *Nature Geosci*, 9, 38–41,
 935 <https://doi.org/10.1038/ngeo2602>, 2016.
- 936 Wang, S., Song, S., Zhang, H., Yu, L., Jiao, C., Li, C., Wu, X., Zhao, W., Best, J.,
 937 Roberts, P., and Fu, B.: Anthropogenic impacts on the Yellow River Basin, *Nat Rev
 938 Earth Environ*, 6, 656–671, <https://doi.org/10.1038/s43017-025-00718-2>, 2025.
- 939 Wang, T., Teng, F., and Zhang, X.: Assessing global and national economic losses from
 940 climate change: a study based on CGEM-IAM in China, *Clim. Change Econ.*, 11,
 941 2041003, <https://doi.org/10.1142/S2010007820410031>, 2020b.
- 942 Wang, Y., Zhao, W., Wang, S., Feng, X., and Liu, Y.: Yellow River water rebalanced by
 943 human regulation, *Sci Rep*, 9, 9707, <https://doi.org/10.1038/s41598-019-46063-5>, 2019.
- 944 Wei, Z., Jian, Z., Sun, Y., Pan, F., Han, H., Liu, Q., and Mei, Y.: Ecological sustainability
 945 and high-quality development of the Yellow River Delta in China based on the
 946 improved ecological footprint model, *Sci Rep*, 13, 3821,
 947 <https://doi.org/10.1038/s41598-023-30896-2>, 2023.
- 948 Wells, C. D., Blanz, B., Ramme, L., Breier, J., Callegari, B., Muralidhar, A., Rajah, J.
 949 K., Lindqvist, A. N., Eriksson, A. E., Schoenberg, W. A., Köberle, A. C., Wang-
 950 Erlandsson, L., Mauritzen, C., Grimeland, M. B., and Smith, C.: The representation of
 951 climate impacts in the FRIDA v2.1 Integrated Assessment Model, *Geoscientific Model
 952 Development*, 19, 1229–1260, <https://doi.org/10.5194/gmd-19-1229-2026>, 2026.
- 953 Wu, J. and Gao, X.: Agridded daily observation dataset over China region and
 954 comparison with the other datasets, *Chinese Journal of Geophysics*, 56, 1102–1111,
 955 <https://doi.org/10.6038/cjg20130406>, 2013.
- 956 Wu, X., Yan, Z., Yang, H., Wang, S., Zhang, H., Shen, Y., Song, S., Liu, Y., Guo, Y.,
 957 Yang, D., and Fu, B.: Ecological restoration in the Yellow River Basin enhances
 958 hydropower potential, *Nat Commun*, 16, 2566, <https://doi.org/10.1038/s41467-025->

959 57891-7, 2025.

960 Wu, Z., Li, Y., Wang, R., Xu, X., Ren, D., Huang, Q., Xiong, Y., and Huang, G.:
961 Evaluation of irrigation water saving and salinity control practices of maize and
962 sunflower in the upper Yellow River basin with an agro-hydrological model based
963 method, *Agricultural Water Management*, 278, 108157,
964 <https://doi.org/10.1016/j.agwat.2023.108157>, 2023.

965 Xu, S., Wang, R., Gasser, T., Ciais, P., Peñuelas, J., Balkanski, Y., Boucher, O., Janssens,
966 I. A., Sardans, J., Clark, J. H., Cao, J., Xing, X., Chen, J., Wang, L., Tang, X., and Zhang,
967 R.: Delayed use of bioenergy crops might threaten climate and food security, *Nature*,
968 609, 299–306, <https://doi.org/10.1038/s41586-022-05055-8>, 2022.

969 Xu, W., Xiao, Y., Zhang, J., Yang, W., Zhang, L., Hull, V., Wang, Z., Zheng, H., Liu, J.,
970 Polasky, S., Jiang, L., Xiao, Y., Shi, X., Rao, E., Lu, F., Wang, X., Daily, G. C., and
971 Ouyang, Z.: Strengthening protected areas for biodiversity and ecosystem services in
972 China, *Proc. Natl. Acad. Sci. U.S.A.*, 114, 1601–1606,
973 <https://doi.org/10.1073/pnas.1620503114>, 2017.

974 Xu, X., Liu, J., Zhang, S., Li, R., Yan, C., and Wu, S.: China land use remote sensing
975 monitoring dataset, <https://doi.org/10.12078/2018070201>, 2018.

976 Yan, Z., Wang, T., Ma, T., and Yang, D.: Water-carbon-sediment synergies and trade-
977 offs: Multi-faceted impacts of large-scale ecological restoration in the Middle Yellow
978 River Basin, *Journal of Hydrology*, 634, 131099,
979 <https://doi.org/10.1016/j.jhydrol.2024.131099>, 2024.

980 Yang, D., Shao, W., Yeh, P. J.-F., Yang, H., Kanae, S., and Oki, T.: Impact of vegetation
981 coverage on regional water balance in the nonhumid regions of China, *Water Resources*
982 *Research*, 45, <https://doi.org/10.1029/2008WR006948>, 2009.

983 Yang, Z., Li, Q., Xue, W., and Xu, Z.: Impacts of nature reserves on local residents’
984 income in China, *Ecological Economics*, 199, 107494,
985 <https://doi.org/10.1016/j.ecolecon.2022.107494>, 2022.

986 Ye, Q., Liu, Q., Swamy, D., Gao, L., Moallemi, E. A., Rydzak, F., and Eker, S.: FeliX
987 2.0: An integrated model of climate, economy, environment, and society interactions,
988 *Environmental Modelling & Software*, 179, 106121,
989 <https://doi.org/10.1016/j.envsoft.2024.106121>, 2024.

990 Yin, P., Gao, Y., Chen, R., Liu, W., He, C., Hao, J., Zhou, M., and Kan, H.: Temperature-
991 related death burden of various neurodegenerative diseases under climate warming: a
992 nationwide modelling study, *Nat Commun*, 14, 8236, <https://doi.org/10.1038/s41467-023-44066-5>, 2023a.

- 994 Yin, S., Gao, G., Ran, L., Lu, X., and Fu, B.: Spatiotemporal Variations of Sediment
995 Discharge and In-Reach Sediment Budget in the Yellow River From the Headwater to
996 the Delta, *Water Resources Research*, 57, e2021WR030130,
997 <https://doi.org/10.1029/2021WR030130>, 2021.
- 998 Yin, S., Gao, G., Ran, L., Li, D., Lu, X., and Fu, B.: Extreme streamflow and sediment
999 load changes in the Yellow River Basin: Impacts of climate change and human activities,
1000 *Journal of Hydrology*, 619, 129372, <https://doi.org/10.1016/j.jhydrol.2023.129372>,
1001 2023b.
- 1002 Yoon, J., Klassert, C., Selby, P., Lachaut, T., Knox, S., Avisse, N., Harou, J., Tilmant,
1003 A., Klauer, B., Mustafa, D., Sigel, K., Talozzi, S., Gawel, E., Medellín-Azuara, J.,
1004 Bataineh, B., Zhang, H., and Gorelick, S. M.: A coupled human–natural system analysis
1005 of freshwater security under climate and population change, *Proceedings of the*
1006 *National Academy of Sciences*, 118, e2020431118,
1007 <https://doi.org/10.1073/pnas.2020431118>, 2021.
- 1008 YRCCMWR: Yellow River Basin Comprehensive Planning (2012-2030), 2015.
- 1009 YRCCMWR: Yellow River Water Resources Bulletin, 2020.
- 1010 Yu, T., Sun, R., Xiao, Z., Zhang, Q., Liu, G., Cui, T., and Wang, J.: Estimation of Global
1011 Vegetation Productivity from Global LAnd Surface Satellite Data, *Remote Sensing*, 10,
1012 327, <https://doi.org/10.3390/rs10020327>, 2018.
- 1013 Zhang, H., Li, R., Cai, X., Zheng, C., Liu, L., Liu, M., Zhang, Q., Lin, H., Chen, L.,
1014 and Wang, X.: Do electricity flows hamper regional economic–environmental equity?,
1015 *Applied Energy*, 326, 120001, <https://doi.org/10.1016/j.apenergy.2022.120001>, 2022a.
- 1016 Zhang, Q., Gu, X., Singh, V. P., Kong, D., and Chen, X.: Spatiotemporal behavior of
1017 floods and droughts and their impacts on agriculture in China, *Global and Planetary*
1018 *Change*, 131, 63–72, <https://doi.org/10.1016/j.gloplacha.2015.05.007>, 2015.
- 1019 Zhang, T., Su, X., Zhang, G., Wu, H., and Liu, Y.: Projections of the characteristics and
1020 probability of spatially concurrent hydrological drought in a cascade reservoirs area
1021 under CMIP6, *Journal of Hydrology*, 613, 128472,
1022 <https://doi.org/10.1016/j.jhydrol.2022.128472>, 2022b.
- 1023 Zhou, F., Bo, Y., Ciais, P., Dumas, P., Tang, Q., Wang, X., Liu, J., Zheng, C., Polcher,
1024 J., Yin, Z., Guimberteau, M., Peng, S., Otle, C., Zhao, X., Zhao, J., Tan, Q., Chen, L.,
1025 Shen, H., Yang, H., Piao, S., Wang, H., and Wada, Y.: Deceleration of China’s human
1026 water use and its key drivers, *Proceedings of the National Academy of Sciences*, 117,
1027 7702–7711, <https://doi.org/10.1073/pnas.1909902117>, 2020.
- 1028 Zhu, Y., Jia, X., Qiao, J., and Shao, M.: What is the mass of loess in the Loess Plateau

1029 of China?, Science Bulletin, 64, 534–539, <https://doi.org/10.1016/j.scib.2019.03.021>,
1030 2019.

1031